

## CHAPTER 6: Geophysical Data for the Hosgri Fault Zone

### TABLE OF CONTENTS

	<b>Page</b>
Lists of Tables, Figures, and Appendices .....	2
Abbreviations and Acronyms .....	3
1.0 INTRODUCTION .....	5
1.1 Marine Seismic-Reflection/ Seismic-Refraction Surveys .....	6
1.2 High-Energy Seismic Surveys .....	7
1.2.1 Western Geophysical Company .....	7
1.2.2 COMAP Alaska 1986 CDP Survey .....	8
1.2.3 PG&E/EDGE Survey .....	8
1.2.4 CCCSIP HESS Program .....	9
1.3 Low-Energy Seismic Surveys .....	10
1.3.1 USGS Low-Energy Seismic Surveys .....	10
1.3.2 PG&E CCCSIP .....	11
2.0 POTENTIAL FIELD DATA—GRAVITY AND MAGNETICS .....	12
2.1 Constraints on the Fault Geometry .....	12
2.2 Hosgri Fault .....	13
3.0 SEISMICITY .....	14
3.1 Earthquake Locations .....	14
3.2 Seismicity of the Hosgri Fault Zone .....	15
4.0 CONCLUSION .....	17
5.0 REFERENCES .....	19

## LISTS OF TABLES, FIGURES, AND APPENDICES

### Tables

Table 1-1 Summary of Hosgri Fault Zone Geometry

### Figures

Figure 1-1 Map Showing the Structural Trend of the HFZ and the Location of LESS and HESS Seismic-Reflection and Potential Field Profiles

Figure 1-2 HESS Profile A-A'

Figure 1-3 USGS 2D LESS Profile PBS-049 and HESS Profile B-B'

Figure 1-4 USGS 2D LESS Profile PBS-043 and HESS Profile C''-C'''

Figure 1-5 USGS 2D LESS Profile PBS-021 and HESS Profile D-D'

Figure 1-6 USGS 2D LESS Profile PBS-026 and HESS Profile E-E'

Figure 1-7 HESS Profile F-F'

Figure 1-8 USGS 2D LESS Profile PBS-047a and HESS Profile G-G'

Figure 1-9 HESS Profile C-C' (Part of PG&E Profile PGE-1)

Figure 1-10 HESS Profile H-H' (Part of PG&E Profile PGE-3)

Figure 1-11 Proposed Track Lines for the PG&E CCCSIP HESS

Figure 2-1 Potential Field Maps for California Coastal Region

Figure 2-2 Gravity and Magnetic Model Cross Section I-I' (Estero Bay)

Figure 2-3 Gravity and Magnetic Model Cross Section J-J' (Point Sal)

Figure 3-1 Earthquake Locations and Single-Event Earthquake Focal Mechanisms along the Central Coast Ranges

Figure 3-2 Hosgri Seismicity Depth Sections A-A' and B-B'

Figure 4-1 Seismicity in Relation to Depth of 3D/2D Seismic Reflection and Potential Field Imaging

### APPENDICES

Appendix A Central Coastal California Seismic Imaging Project—Environmental Review, Permitting, and Baseline Monitoring

## ABBREVIATIONS AND ACRONYMS

1D	one-dimensional
2D	two-dimensional
3D	three-dimensional
CCC	California Coastal Commission
CCCSIP	Central Coastal California Seismic Imaging Project
CCSN	Central Coast Seismic Network
CDP	common depth point
CEQA	California Environmental Quality Act
CISN	California Integrated Seismic Network
CSLC	California State Lands Commission
DCPP	Diablo Canyon Power Plant
HARC	Houston Advanced Research Center
HESS	high-energy seismic survey
HFZ	Hosgri fault zone
HSS	Hosgri–San Simeon–San Gregorio
Hz	hertz
IPRP	Independent Peer Review Panel
kJ	kilojoule
km	kilometer
LESS	low-energy seismic survey
LTSP	Long Term Seismic Program
m	meter
M	magnitude
MBES	multibeam echosounder
mm/yr	millimeters per year
NEPA	National Environmental Policy Act
NRC	U.S. Nuclear Regulatory Commission
OADC	optimal anisotropic dynamic clustering
OBS	ocean bottom seismometer
s	second

TWTT      two-way travel time  
USGS      U.S. Geological Survey

## 1.0 INTRODUCTION

The AB 1632 Report addressed the uncertainty regarding the tectonic setting of the Hosgri Fault Zone (HFZ), as well as experts' disagreement over the fault zone's characterization, as follows:

*The Hosgri fault zone, 4.5 kilometers west of Diablo Canyon, creates the primary seismic hazard at the plant site. Over the years, there has been uncertainty regarding the tectonic setting of this fault zone, and the characterization of the Hosgri as either a lateral strike-slip fault or as a thrust fault. Current published geologic and seismologic research literature, much of which has been developed through PG&E's Long-Term Seismic Program (LTSP) supports the interpretation that the Hosgri fault is predominantly characterized by strike-slip faulting. Experts with the U.S. Geological Survey, the California Geological Survey, and the Southern California Earthquake Center have accepted the strike slip characterization for the Hosgri Fault. However, a minority of scientists disagrees with this characterization and believes the Hosgri Fault is a thrust fault.*

Both the dip of the HFZ offshore of the DCPD and its interactions between the the San Simeon and Shoreline fault zones were identified by the Central Coastal California Seismic Imaging Project (CCCSIP) and the California Public Utility Commission's Independent Peer Review Panel (IPRP) as high-priority targets for investigation. This chapter reviews geophysical data related to the HFZ that have been collected or published since the original Long Term Seismic Program (LTSP) report (PG&E, 1988a) was issued.

The CCCSIP database consists of a variety of geologic and geophysical data, including multibeam echosounder (MBES) bathymetry, low-energy shallow-penetration seismic-reflection profiles from the U.S. Geological Survey (USGS) 2008 and 2009 surveys, high-energy deep-penetration seismic-reflection profile data from the PG&E geophysical survey legacy data archive, 2D seismic-reflection profile data from the 3D low-energy seismic survey (LESS) study offshore of Point Buchon (PG&E, 2014), and LTSP maps and data (PG&E, 1988a, b; Willingham et al., 2013). Supplementary data provided to PG&E by the USGS include potential field (magnetic and gravity) anomaly maps (Sliter et al., 2009; Johnson and Watt, 2012; Langenheim, 2013; Langenheim et al., 2013), and earthquake hypocenters and focal mechanisms (Hardebeck, 2010, 2013, 2014).

The HFZ trends subparallel to the south-central California coast for over 110 kilometers (km) from south of Purisima Point to north of Point Estero and forms the eastern margin of the present offshore Santa Maria Basin (see Figure 1-1; PG&E, 1988a; Willingham et al., 2013). The HFZ is considered part of the coastal California fault system that also includes the San Simeon and San Gregorio fault zones to the north (Hall, 1975; Graham and Dickinson, 1978; Silver and Normark, 1978; Dickinson et al., 2005) and is the most studied (PG&E, 1988a) segment of the Hosgri–San Simeon–San Gregorio fault system to date.

Published interpretations for Quaternary slip on the HFZ have included reverse-slip (Namson and Davis, 1990), thrust and reverse-slip (Crouch et al., 1984), and strike-slip (PG&E, 1988a; Hall et al., 1994; Hanson and Lettis, 1994; Steritz and Luyendyk, 1994;

Willingham et al., 2013). Hanson et al. (2004) present a comprehensive review of the style and rate of Quaternary deformation of the HFZ using geologic and geophysical data acquired as part of the LTSP (PG&E, 1988a). Analysis of geomorphic and structural features along its entire length shows that the HFZ is characterized as an active 110 km long convergent, right-oblique slip (transpressional) fault zone with identifiable northern and southern terminations (Willingham et al., 2013). The role of the HFZ as an uplift rate boundary for the Irish Hills is discussed in Chapter 12.

Estimates of cumulative strike-slip offset along the Hosgri–San Simeon–San Gregorio (HSS) fault system range from 5 km or less (Sedlock and Hamilton, 1991; Sorlien et al., 1999; Underwood and Laughland, 2001) to 80–185 km (Hall, 1975; Graham and Dickinson, 1978; Clark et al., 1984; Jachens et al., 1998; Dickinson et al., 2005; Burnham, 2009). Correlation of offset geologic terranes and associated magnetic anomalies by Langenheim et al. (2013) suggests that right-lateral offset of the HSS fault is not constant along the entire fault system, but instead increases northward from nearly zero offset south of Point Arguello to approximately 155 km offset to the north between Cape San Martin and Año Nuevo Point. This pattern of northward increasing offset in pre-Neogene and Neogene rocks is consistent with a northward increase in Quaternary slip rates as well: 0.5–2 millimeters per year (mm/yr) between Point Sal and Point Arguello (Hanson et al., 2004); 1–3 mm/yr at San Simeon (Hanson et al., 2004); and 4–11 mm/yr at Año Nuevo (Weber, 1994). The pattern of northward increasing right-lateral displacement on the HSS can be explained in part by left transfer of right-lateral displacement onto this fault system from subsidiary faults east of the HSS fault zone system (Lettis et al., 2004).

The improved resolution and quality of these recent geologic and geophysical studies has reduced much of the uncertainty regarding the tectonic setting of the HFZ and its characterization as either a strike-slip or a thrust fault. The following sections review and integrate the LTSP-era data and more recent marine seismic-reflection, potential field, and seismicity (earthquake) data collected along the HFZ to examine constraints on the dip of the fault zone in the vicinity of the DCP.

## **1.1 Marine Seismic-Reflection/ Seismic-Refraction Surveys**

Because the HFZ lies offshore, the mapping of this feature has been based primarily on the analysis of marine seismic-reflection data. Willingham et al. (2013) reviewed the seismic exploration history of the fault zone. Petroleum exploration of the study area (part of the offshore Santa Maria Basin) began in the 1960s with regional seismic-reflection profiling, gravity, and magnetic surveys. Hoskins and Griffiths (1971) first published evidence of a major fault offshore of the south-central California coast that was later defined in more detail based on a USGS seismic-reflection survey showing that the HFZ exhibited seafloor expressions. The fault name “Hosgri” is a contraction of the Hoskins and Griffiths names (Wagner, 1974).

In the early 1970s, PG&E began construction and licensing processes for the DCP. The existence of the HFZ approximately 4 km offshore prompted high-resolution seismic-reflection surveys by the USGS and PG&E to better define the limits, near-surface

characteristics, and recency of activity of the fault zone. The USGS-sponsored investigations of the Central California continental shelf in 1972 and 1973 indicated that lateral displacements were associated with the HFZ (Wagner, 1974). In 1973 and 1974, PG&E collected over 1,300 km of high-resolution seismic-reflection data, much of it within this study area. Leslie (1981) used USGS data from the 1970s, and PG&E data collected in 1973 and 1974 to study the northern termination of the HFZ in the nearshore area north of Estero Bay. PG&E also acquired selected higher-energy survey lines from the USGS and geophysical exploration contractors. However, the deeper-penetration exploration lines were generally acquired along a regional grid with wide spacing, and many of the lines terminated too far from the coast to provide good images of the HFZ. As a result, the character of the fault zone at depth was nondescript and could not be used to differentiate between the varieties of tectonic models being proposed for the region.

## **1.2 High-Energy Seismic Surveys**

PG&E purchased a number of proprietary seismic-reflection data sets and also collected new seismic-reflection data as part of the LTSP in the 1980s. High-energy acoustic sources include air guns and water guns with volumes greater than 10 cubic inches (in<sup>3</sup>), and sparkers with energies greater than 2 kilojoules (kJ). Review of the seismic-reflection profiles produced with these acoustic sources by Willingham et al. (2013) showed the HFZ to be steeply dipping (>60°) to subvertical in attitude. Figure 1-1 shows the location of the moderate- to high-energy 2D seismic-reflection profiles discussed in the following sections.

### **1.2.1 Western Geophysical Company**

In the mid-1980s, PG&E purchased 570 km of proprietary high-energy seismic-reflection survey data from the Western Geophysical Company (now WesternGeco, the geophysical survey business unit of Schlumberger Limited). These data were originally collected in 1974, 1975, and 1982 and extended from north of Piedras Blancas Point to south of Point Sal. The Western Geophysical data were collected primarily in federal waters, but the HFZ was crossed in places near the distal edge of the continental shelf. The data were collected using air-gun arrays and processed to 46- to 60-fold stacks and migrated. Record length was 6.0 s. The interpretation of these data was integrated with the 1970's PG&E data and presented in the LTSP documentation (PG&E, 1988a, 1990) and in the study by Willingham et al. (2013).

Profile A-A' (on Figure 1-2) shows the eastern and western traces of the HFZ offshore Cambria, immediately north of the San Simeon-Hosgri pull apart basin (Half Graben fault zone discussed in Chapter 4). Both traces are vertical in the upper one second of the record, but they dip to the northeast at depth. Willingham et al. (2013) interpret the western trace to be the main fault of the HFZ at this location. Profile B-B' (Figure 1-3b) crosses the HFZ south of Point Estero near where the Half Graben fault zone begins to deviate from the HFZ (Lettis et al., 1990; Hanson et al., 2004; Chapter 4 of this report). Two near vertical traces are imaged. The main trace near shot point 100 offsets sedimentary layers up to the time of the post-Wisconsin unconformity (<10,000 y bp) and exhibits a steep dip to a depth of 2.5 s two-way travel time (TWTT; ~2–3 km). The

profile also indicates about 1 km of vertical, southwest side down displacement across the HFZ at this location.

### **1.2.2 COMAP Alaska 1986 CDP Survey**

In 1986, PG&E contracted with COMAP Alaska to conduct a multichannel moderate-energy seismic-reflection survey (MESS) of the California state waters area from Cape San Martin in the north to San Luis Obispo Bay in the south. The objective of the survey was to provide additional control for mapping of the HFZ zone in the relatively shallow-water nearshore areas. Approximately 500 km of primary survey lines were run perpendicular to the trend of the HFZ using a 160-in.<sup>3</sup>) water gun and a 48-channel hydrophone streamer. The data were recorded for 2 seconds (s). These data are used in Chapters 3 in conjunction with 2D and 3D LESS data to map the southern extension of the Shoreline fault zone in San Luis Obispo Bay, as well as in Chapter 4 to review the evidence for a step-over between the Hosgri and San Simeon fault zones north of Estero Bay.

Profiles C'' -C''', D-D' , E-E' , F-F' , and G-G' (Figures 1-4 b through 1-8b) are located north and south of the DCP, between Estero Bay and Point San Luis. These profiles show two traces of the HFZ that are near vertical in the upper 1.0–1.5 s (1–1.4 km) of the record and have a steep northeasterly dip (~60°–75°) below that depth. .

### **1.2.3 PG&E/EDGE Survey**

In 1986, the PG&E/EDGE deep crustal seismic experiment acquired 590 km of deep-crustal-reflection common-depth-point (CDP) lines, as well as onshore-offshore seismic-refraction data (Ewing and Talwani, 1991; Meltzer and Levander, 1991; Trehu, 1991; Howie et al., 1993). The PG&E/EDGE field program was an academic and industrial consortium formed to study the continental margin of North America, located at Rice University's Houston Advanced Research Center (HARC). A series of six profiles were shot by Digicon for PG&E, HARC, and Rice University using a 6,000 in.<sup>3</sup> air-gun array and a 4,500 m long, 180-channel hydrophone streamer. Records were 45-fold with a 16 s record length. Profiles extended perpendicular to the coast, from the base of the continental slope to the continental shelf, as well as parallel to the axis of the Santa Maria Basin.

The most significant crustal-scale feature observed in the EDGE profiles was a continuous deep reflection at approximately 6 s TWTT that is interpreted to represent subducted oceanic crust, a remnant of the Farallon Plate. The reflection is approximately 6 km deep at the base of the continental slope and dips 8 degrees towards the coast to a depth of 14–16 km beneath the Santa Maria Basin. There the deep reflection breaks into a series of dipping reflections, suggesting that the oceanic crust is imbricated at that point (Meltzer and Levander, 1991; Trehu, 1991). The remnant oceanic crust is interpreted to act as a detachment surface above which shallow (<15 km) strike-slip and reverse faults are imaged.

North of the DCP, in Estero Bay, Profile C-C' (part of Line PGE-1 on Figure 1-9) shows the main fault trace of the HFZ as vertical to depths of 2 s (~3 km). Two splay



faults branch from the main trace at approximately 1.7 s. Farther south in San Luis Obispo Bay, Profile H-H' (part of Line PGE-3 on Figure 1-10) shows the main trace of the HFZ to be near vertical to 3 s (~4–5 km), with a slight northeast dip below 2.4 s. The single trace branches into a flower structure that produces a 3 km wide zone of disruption above 1 s. Flower structures, or the upward divergence of subsidiary splay faults, are diagnostic of transpressional and transtensional strike-slip fault systems. In contrast to the Santa Maria Basin, west of the HFZ, the shallow geology on the continental shelf, east of the HFZ, is not as well imaged in Profiles C-C' and H-H' due to the use of a low frequency (15-60 Hz) energy source and large hydrophone group spacing (25 m). McIntosh et al. (1991) mapped the HFZ on Line RU-3 (parallel to line PGE-3) as a set of steeply inclined (>50°) fault strands and low-angle thrusts. The vertical, southwest side down separation across the HFZ is at least 1.7 s (~2,000 m) at this location.

The suggestion that the HFZ may be a thrust fault system prompted a number of investigators to reprocess the EDGE seismic-reflection data to improve the imaging of steeply dipping structures that exist in the presence of large lateral velocity contrasts across the fault zone. Advances in seismic-reflection data processing technology during the late 1980s and early 1990s were applied to address coherent out-of-plane energy that was observed as conflicting dip directions in the profiles. A full pre-stack depth migration of Line RU-3 shows the HFZ to have a 75-degree east dip (Lafond and Levander, 1993). Additional studies by Worden (1992), Pullammanappallil and Louie (1994), Shih and Levander (1994), Steritz and Luyendyk (1994), and Honjas et al. (1995) have all concluded that the HFZ is near vertical to steeply northeast dipping. None of these data point to the flattening of the HFZ with depth; in addition, the data are in agreement with PG&E/EDGE results that the HFZ is steeply dipping to subvertical (Miller and Meltzer, 1999).

Both the EDGE and COMAP surveys represent some of the last high-energy seismic-reflection surveys (HESS) permitted in California state waters. In 1987, the California State Lands Commission (CSLC) determined that permits for high-energy geophysical surveys employing air guns could not be issued unless, and until an Environmental Impact Report was certified by the CSLC.

#### **1.2.4 CCCSIP HESS Program**

As part of the response to the AB 1632 Report recommendation to use “three-dimensional geophysical seismic reflection mapping and other advanced techniques to explore fault zones near Diablo Canyon,” PG&E applied for permits to conduct 3D HESS investigations offshore of the DCP in 2011. The CCCSIP HESS program was designed to provide deeper imaging of the San Simeon–Hosgri–Shoreline–Los Osos fault system using two 1,650 in.<sup>3</sup> air-gun strings with four 6 km long, 480-channel hydrophone streamers and modern 3D seismic-reflection acquisition and processing technology. The MBES data and potential field (gravity and magnetics) data to constrain the seismic-reflection signal migration and crustal structure models were to be collected as well. The four proposed HESS survey areas, or racetracks, are shown on Figure 1-11.

The process to obtain the necessary permits and approvals for the proposed HESS investigation followed the procedures contained in the 1999 *High Energy Seismic Survey Review Process and Interim Operational Guidelines for Marine Surveys Offshore Southern California* (“HESS Guidelines”; High Energy Seismic Survey Team, 1999). The proposed survey area overlapped state and federal waters and required multi-agency review and coordination for the necessary California Environmental Quality Act (CEQA) and National Environmental Policy Act (NEPA) reviews of the project. Appendix A summarizes the environmental review, permitting, and baseline monitoring activities that were conducted.

The scope and duration of the proposed HESS survey areas was subsequently reduced based on input from the California Public Utility Commission’s IPRP (2012a, 2012b) and concerns by environmental agencies and groups about the potential impacts of the project on fish, marine invertebrates, and marine mammals. The CSLC certified the Environmental Impact Report and issued a Marine Geophysical Survey Permit to PG&E in August 2012 for a maximum of three survey areas (Boxes 1, 2, and 4 on Figure 1-11). The surveys were to be conducted during the winter hiatus in whale migration along the Central California coast, October 15 through December 31. The California Coastal Commission (CCC) considered a modified scope for the project consisting of one survey area in Estero Bay (Box 4 on Figure 1-11) in order to evaluate the likelihood of successful seismic imaging and the effectiveness of the proposed comprehensive environmental monitoring and mitigation program. The CCC ultimately denied the PG&E’s Coastal Development Permit in November 2012, citing concerns about the potential environmental impact of using air guns in shallow coastal waters.

### **1.3 Low-Energy Seismic Surveys**

Low-energy geophysical survey equipment authorized for use by the CSLC in state waters includes sub-bottom profilers, echosounders, and side-scan sonar and passive systems (magnetometers and gravimeters). Sub-bottom profilers with outputs less than 2 kJ include mini-sparkers and boomers and higher-frequency chirp systems. Low-energy acoustic sources provide higher-resolution imagery than high-energy sources but are limited to shallow depths (hundreds of meters versus kilometers). Low-energy data are used to assess the surface location and recency of activity along faults, as well as map bathymetry, Quaternary unconsolidated sediment distribution and thickness, and bedrock outcrop areas.

#### **1.3.1 USGS Low-Energy Seismic Surveys**

In 2008 and 2009, the USGS conducted LESS single-channel high-resolution surveys in this study area as part of the California State Waters Mapping Program (Sliter et al., 2009). Although this was a low-energy survey (<2 kJ), it was apparently the first seismic-reflection data collected in the San Simeon–Estero Bay offshore area since the 1987 limitations on seismic survey energy levels in California state waters (see discussion in Section 1.2.3). A total of 1,500 km of low-energy single-channel seismic-reflection data were collected at 800 m line spacing, with additional lines providing a 400 m spacing in selected areas. Johnson and Watt (2012) used these data to document the location, length,

and continuity of multiple fault strands in order to highlight fault zone heterogeneity and demonstrate the impact that variations in fault trend have on the formation of shallow structures and tectonic geomorphology. The USGS 2D LESS profiles that coincide with, or are located near, the deep-penetration CDP profiles discussed elsewhere in this chapter are shown on Figures 1-1, 1-3 through 1-6, and 1-8. These shallow-penetration LESS seismic-reflection profiles all image steeply dipping strands of the HFZ in the upper 200 to 300 m and provide near-surface control on the location and offset of deeper fault zones imaged with the HESS data.

### ***1.3.2 PG&E CCCSIP***

PG&E collected 3,255 line km of high-resolution 2D and 3D LESS seismic-reflection profile data in 2011 and 2012 in response to the AB 1632 Report recommendation to conduct 3D seismic-reflection studies. Approximately 60 km<sup>2</sup> of full-fold 3D data are reported in Chapters 2 and 3 and were used to map the location and constrain the sense of slip and the slip rate of the Hosgri and the Point Buchon-Shoreline fault zones.

## 2.0 POTENTIAL FIELD DATA—GRAVITY AND MAGNETICS

Potential field (gravity and magnetic) data available at the time of the original LTSP (e.g. McCulloch and Chapman, 1977; Beyer and McCulloch, 1988; Chapman et al., 1989) had insufficient resolution for detailed characterization of the HFZ. Residual magnetic intensity data offshore of the DCP, presented in LTSP Plate Q43m-2 (PG&E, 1988b), were collected in 1976 with a flight line spacing of 1 mile (1.6 km) at an altitude of 610 m (2,000 feet) above sea level. These data were used primarily in identifying changes in basement rock characteristics and morphology and in confirming seismic-reflection data interpretation of basement structures.

New aeromagnetic and gravity data were collected by the USGS (Langenheim, 2013; Langenheim et al., 2013) to examine the dip, depth, extent, and cumulative offsets of the HSS fault system. Langenheim et al. (2013) used 25,000 gravity measurements to create an isostatic residual gravity map of the central coastal region (see Figure 2-1a). The isostatic correction removes the long-wavelength effect of deep crustal and/or upper mantle masses that support regional topography. The onshore data density in the vicinity of the DCP is one station per 2 km<sup>2</sup>; the offshore data density is variable and plotted from gridded compilations of shipboard gravity data.

New aeromagnetic and marine magnetic data collected since the LTSP have improved resolution at both regional and local scales within the study area (see Figure 2-1b). Magnetic anomalies reflect the abundance of magnetic minerals, primarily magnetite, in rocks from the surface to mid- to lower-crustal depths. In the Coast Ranges, these anomalies are generally associated with Mesozoic basement rocks. Aeromagnetic surveys were flown at a nominal height of 150–305 m above ground along flight lines that were spaced 530–800 m apart (Langenheim et al., 2009). A high-resolution helicopter magnetic survey was conducted along the coast between Point Buchon and Point San Luis at 50 m elevation along 150 m spaced lines (Langenheim et al., 2012); marine magnetic data were collected at 400 m line spacing (Sliter et al., 2009; Watt et al., 2011).

### 2.1 Constraints on the Fault Geometry

Potential field constraints on fault geometry (e.g., fault dip) are derived primarily from magnetic field data. The edges of displaced magnetic rock bodies were defined using a maximum horizontal gradient method. Gradient maxima occur directly over vertical or near-vertical contacts that separate rocks of contrasting magnetization. High-resolution magnetic surveys of the DCP site area were used to constrain the geometry of the Shoreline fault zone (PG&E, 2011; Watt, 2012). Isostatic gravity anomalies reflect density variations in the upper 10–15 km of the crust and were used by Langenheim et al. (2013) to constrain HFZ dips in the upper 2–3 km of the crust. Crustal profiles of potential field data are based on a 2½-dimensional simultaneous gravity/magnetic inversion program that was initially constrained by mapped geologic relationships, physical property (magnetic susceptibility and density) measurements, and well data (Langenheim et al., 2013).

## 2.2 Hosgri Fault

The HFZ marks a significant potential field (magnetic and gravity) boundary along the edge of the continental shelf and defines the western boundary of the Los Osos domain (see Figure 2-1). The Hosgri fault separates more westerly trending magnetic anomalies to the east on the continental shelf from more northerly trending anomalies to the west in the Santa Maria Basin. Offshore Estero Bay, the HFZ lies at the base of a steep gravity gradient that extends for a distance of approximately 70 km between San Simeon and Point Sal. The gradient is consistent with a steep northeast-dipping fault, northeast-side-up. The Langenheim et al. (2013) preferred Hosgri model for Profile I-I' in Estero Bay has a steep northeast dip of 65–70 degrees in the upper 3 km and a vertical dip to 8 or 15 km depth, depending on basement magnetic properties (Figure 2-2). Farther south at Point Sal, magnetic data indicate a near-vertical HFZ that dips 80–85 degrees northeast and extends to a depth of 10 km (Profile J-J' on Figure 2-3). Nearby marine seismic-reflection Profiles B-B' and C-C' in Estero Bay (Figures 1-3 and 1-9) and H-H' near Point Sal (Figure 1-10) indicate similar geometries at shallower depths (< 6 km).

### 3.0 SEISMICITY

Seismicity (earthquake) data provide critical constraints on both the geometry (strike and dip) and sense of motion (rake) of seismogenic faults. Seismicity alignments in two and three dimensions are used to determine fault geometry. Earthquake first-motion focal mechanisms provide information about the type of faulting, the direction of slip (rake) on the fault plane, and the orientation of principal stresses.

McLaren and Savage (2001) summarized the seismographic station coverage in the Central Coast region. Aside from early instrumentation installed in 1927 in Santa Barbara and in 1961 at Parkfield, there were very few instruments in this region until the 1980s. As a result, the few earthquakes that were recorded during this period had large location uncertainties and could not be confidently associated with individually mapped faults. Seismograph station coverage in the coastal region improved in the early 1980s with the addition of Northern California Seismic Network (NCSN) stations as part of the National Earthquake Hazards Reduction Program (Lindh et al., 1981). In 1987, PG&E established a 20-station Central Coast Seismic Network (CCSN) as part of the LTSP (McLaren and Savage, 2001). The CCSN extends approximately 30 km along the coastline from Ragged Point south to Point Sal. Starting in 2006, PG&E began a five-year program to update the original 20 stations with digital telemetry and digital recorders for velocity and acceleration (six components). There are now 16 digital stations in the CCSN (14 station upgrades and 2 new stations). The recorded data are markedly improved and result in more accurate earthquake locations, particularly in the offshore region. PG&E installed ocean-bottom seismometers in 2013 to further improve offshore locations (Chapter 5).

#### 3.1 Earthquake Locations

McLaren and Savage (2001) examined the first 10 years (1987–1997) of seismicity data from the CCSN. They used the joint hypocenter-velocity inversion program, VELEST (Roecker, 1981) to invert P-wave arrival times for a one-dimensional (1D) flat-layer velocity model, derive a S-wave model from the P-wave model, and estimate corresponding P- and S-wave station corrections and the HYPOINVERSE program (Klein, 1989) for the final earthquake locations. Analysis of over 1,000 earthquake locations and 212 well-constrained focal mechanism solutions indicated that seismicity coincided with mapped Quaternary faults and areas of tectonic uplift. Comparison of network data with larger ( $M > 5$ ) historic seismicity indicated a persistent spatial distribution of seismic activity in the area.

Following the 2003 M 6.5 San Simeon earthquake, Hardebeck (2010) examined 20 years (1987–2008) of earthquake data for the Coast Ranges study region, including data from the original CCSN and more recent data from the California Integrated Seismic Network (CISN). Hardebeck (2010) relocated approximately 16,000 earthquakes (including aftershocks of the 2003 San Simeon earthquake) using waveform cross-correlation differential times and the catalog arrival time picks using the double-difference programs hypoDD (Waldhauser and Ellsworth, 2000) and tomoDD (Zhang and Thurber, 2003).

The regional 3D model represents an improvement with respect to the earlier 1D model of McLaren and Savage (2001). The most noticeable improvement is in the offshore region near San Luis Obispo, between the coastline and the HFZ. The lack of seismograph station coverage west of the coastline (i.e., offshore), however, results in location uncertainties that are greatest in the direction perpendicular to the coastline. The Point Buchon ocean bottom seismometer (OBS) array (Chapter 5) was installed by PG&E in 2013 to improve earthquake location accuracy in the area.

## 3.2 Seismicity of the Hosgri Fault Zone

Earthquake epicenters and focal mechanisms for the region surrounding the DCPD are shown in Figure 3-1. The section of the HFZ between Estero Bay and Point San Luis is the most microseismically active portion of the HFZ (McLaren and Savage, 2001). The HFZ enters into a left-restraining bend in the region north of Point San Luis and is characterized by two parallel surface traces that dip steeply to the northeast (Figures 1-6 and 1-7; Johnson and Watt, 2012; Willingham et al., 2013). North of Point Buchon (35.25° N), the surface expression of the western HFZ trace terminates and lateral fault slip (and microseismicity) is transferred to the eastern HFZ trace through a releasing step-over.

Single event and composite focal mechanisms along the HFZ, between Estero Bay and Point San Luis, are consistent with right-lateral strike-slip motion on a near-vertical plane aligned with the strike of the HFZ (McLaren and Savage, 2001; Hardebeck, 2010). The focal mechanisms shown on Figure 3-1 are from Hardebeck (2010) using the program HASH (Hardebeck and Shearer, 2002) and from the USGS catalog using the algorithm FPFIT (Reasenber and Oppenheimer, 1985). FPFIT uses P-wave first-motion data from earthquakes located with a 1-D velocity model and includes only those earthquakes with unique, good-quality solutions that use 25 or more P-wave first motions and that have converged to the solution by finding the minimum misfit solution. HASH computes P-wave first-motion focal mechanisms using takeoff angles observed from ray tracing in the 3-D seismic velocity model. HASH assigns mechanism quality (A, B, C, and D) based on the solution stability with respect to the uncertainty in the take-off angles and polarity observations. Quality D mechanisms are from those earthquakes that did not meet the criteria of Quality A to C earthquakes, but were considered adequate upon examination of the polarity data (at least 6 P-wave first motions) and the computed focal mechanisms (Hardebeck, 2010). The majority of HASH focal mechanisms for the HFZ are assigned a quality of D. Hardebeck (2013) used an optimal anisotropic dynamic clustering (OADC) algorithm (Ouillon et al., 2008), along with composite focal mechanisms to objectively define the geometry of the HFZ. The preferred OADC dip solution for the HFZ ranges between 76 degrees and 89 degrees NE (Hardebeck, 2012).

Profiles A-A' and B-B in Figure 3-2 show the distribution of seismicity with depth parallel, and perpendicular, to the strike of the HFZ, respectively. The maximum depth of seismicity in this area is about 13 km. This depth is above the top of the relic oceanic crust interpreted from the PG&E/EDGE seismic profiles (Section 1.2.3) and is consistent with earthquakes occurring in the brittle upper crust (McLaren and Savage, 2001).

The majority of seismicity along the HFZ between 35.12° N and 35.22° N (the southern half of the rectangle in Figure 3-1 between Point San Luis and Point Buchon) is associated with the western trace of the HFZ (“WHZ” of Johnson and Watt, 2012). These events tend to be relatively shallow (< 6 km, Profile A-A’ Figure 3-2) and exhibit right lateral oblique-strike slip motions along steep northeast dipping fault planes.

The pattern of seismicity north of 35.22° N (the northern half of the rectangle in Figure 3-1 between Point Buchon and Estero Bay) is more complex and includes earthquakes associated with both the HFZ and the Point Buchon-Shoreline fault. Earthquakes located in this area occur over a wider range of depths (A-A’, Figure 3-2) and exhibit a mixture of strike slip and reverse focal mechanisms (Figure 3-1; Hardebeck, 2010). The majority of focal mechanisms associated with the HFZ exhibit right-lateral strike-slip motion parallel to the strike of the HFZ. A number of mechanisms, located between the Hosgri and Point Buchon faults in Figure 3-1 exhibit a reverse-oblique sense of motion and are subparallel to west trending splay faults associated with the Point Buchon fault (Chapter 2).



## 4.0 CONCLUSION

PG&E has addressed the AB 1632 Report's comments about "*uncertainty regarding the tectonic setting of this (Hosgri) fault zone, and the characterization of the Hosgri as either a lateral strike slip fault or as a thrust fault.*" Earlier models by Namson and Davis (1990) and Crouch et al. (1984) that identified the HFZ as a major thrust fault underlying the Coast Ranges are not supported by the high-energy marine 2D seismic-reflection data acquired during the LTSP; nor are they supported by potential field and seismicity data collected during the LTSP Update and CCCSIP program. Geologic observation (Hanson et al., 2004), seismicity data (McLaren and Savage, 2001; Hardebeck, 2010, 2013), and geophysical data (Johnson and Watt, 2012; Langenheim et al., 2013; Willingham et al., 2013) all demonstrate that the HFZ is a right-lateral strike-slip fault that dips steeply (75°–90°) northeast to a depth of 12–14 km in the vicinity of the DCP (see Table 1-1).

Comparison of multiple geophysical data sets on Figure 4-1 shows general agreement, at various scales, in the overall geometry of the HFZ in the vicinity of the DCP; however, the depth of resolution of the fault zone varies with the type of geophysical data used. Seismic-reflection data typically image structure from a depth of few hundred meters (in the case of LESS) to a few kilometers (in the case of HESS), while potential field (magnetic) and seismicity (earthquake) data provide deeper imagery into the crust, extending to a depth of 10–15 km. Additional HESS data do not need to be collected at this time, given the abundance of previously collected HESS data, the limited depth of penetration relative to the dimensions of the fault zone, and the environmental concerns about the use of high-energy seismic surveys.

The intersection of the HFZ with the Point Buchon-Shoreline and San Simeon fault zones is addressed in Chapters 2 and 4. Global examples (e.g., Wesnousky, 2006) suggest that the Hosgri and Point Buchon-Shoreline faults may rupture together given their close proximity in the near surface and at depth (Hardebeck, 2010, 2013). The Shoreline Fault Zone Report concluded that the branching geometry between the Shoreline and Hosgri faults offshore of Point Buchon inhibited joint rupture. Dynamic rupture modeling showed that if rupture on the Hosgri stepped on to the Point Buchon-Shoreline fault, the rupture would continue for only a few kilometers at most. Similarly, ruptures on the Shoreline fault stepping onto the Hosgri fault would continue for only a few kilometers (Kame et al., 2003; PG&E, 2011a, Appendix J). Similarly, Chapter 4 states that while evidence for recent fault rupture between the Hosgri and San Simeon fault zones is not well imaged in some locations, the data do not preclude the existence of fault linkage at seismogenic depths. Chapter 13 presents a ground-motion hazard sensitivity analysis for the linkage of the Hosgri and San Simeon faults, and a combined rupture of the Hosgri–San Simeon and Shoreline faults. These data will be evaluated and integrated into an updated seismic source characterization model for input into the NRC-requested probabilistic seismic hazard update for the DCP.

**Table 1-1. Summary of Hosgri Fault Zone Geometry**

Type of Data	Hosgri Dip Measurements
Seismic Reflection	60°–90° NE dip (1–3 km)
Gravity	Estero Bay 65°–70° NE dip (0–3 km)
Magnetics	Estero Bay Vertical (3–8/15 km) Point Sal 80°–85° NE dip (0–10 km)
Seismicity	Vertical (2–12 km) <sup>1</sup> ; 76°–89° NE dip <sup>2</sup> , 76° ± 13° NE dip <sup>3</sup> ; 180° ± 24° rake <sup>2,3</sup>

<sup>1</sup> Hardebeck (2010)

<sup>2</sup> Hardebeck (2012)

<sup>3</sup> Hardebeck (2013)

## 5.0 REFERENCES

Beyer, L.A., and McCulloch, D.S., 1988. *Free-Air Gravity Anomaly Map of the Offshore Santa Maria Basin*, U.S. Geological Survey Open-File Report 89-322, 1 map, scale 1:125,000.

Burnham, K., 2009. Predictive model of San Andreas Fault system paleogeography, Late Cretaceous to early Miocene, derived from multidisciplinary conglomerate correlations, *Tectonophysics* **464**: 195–258.

Chapman, R.H., Beyer, L.A., and Youngs, L.G., 1989. Bouguer gravity and magnetic anomaly map of the south-central California Continental margin (Map 4c): in Greene H.G. and Kennedy, M.P. (editors), *California Continental Margin Geologic Map Series: South-Central California continental margin—Area 4 of 7*, California Division of Mines and Geology, scale 1:250,000.

Clark, J.C., Brabb, E.E., Greene, H.G., and Ross, D.C., 1984. Geology of Point Reyes peninsula and implications for San Gregorio fault history: in Crouch, J.K., and Bachman, S.B. (editors), *Tectonics and Sedimentation Along the California Margin*, Pacific Sections, Society of Economic Paleontologists and Mineralogists, vol. 38, pp. 67–85.

Crouch, J., Bachman, S.B., and Shay, J.T., 1984. Post-Miocene compressional tectonics along the central California margin: in Crouch, J., and Bachman, S.B. (editors), *Tectonics and Sedimentation Along the California Margin*, Pacific Section, Society of Exploration Paleontologists and Mineralogists, vol. 38, pp. 37–54.

Dickinson, W.R., Ducea, M., Rosenberg, L.I., Greene, H.G., Graham, S.A., Clark, J.C., Weber, G.E., Kidder, S., Ernst, W.G., and Brabb, E.E., 2005. *Net Dextral Slip, Neogene San Gregorio-Hosgri Fault Zone, Coastal California: Geologic Evidence and Tectonic Implications*, Geological Society of America Special Paper 391, 43 pp.

Ewing, J., and Talwani, M., 1991. Marine deep seismic reflection profiles off central California, *Journal of Geophysical Research* **96**: 6423–6433.

Graham, S.A., and Dickinson, W.R., 1978. Evidence for 115 kilometers of right slip on the San Gregorio–Hosgri Fault trend, *Science* **199**: 179–181.

Hall, C.A., 1975. San Simeon–Hosgri Fault System, coastal California: Economic and environmental implications, *Science* **190**: 1291–1293.

Hall, N.T., Hunt, T.D., and Vaughan, P.R., 1994. Holocene behavior of the San Simeon fault zone, south-central coastal California: in Alterman, I., McMullen, R.B., Cluff, L.S., and Slemmons, D.B. (editors), *Seismotectonics of the Central California Coast Ranges*, Geological Society of America Special Paper 292, pp. 167–189.

Hanson, K.L., and Lettis, W.R., 1994. Estimated Pleistocene slip rate for the San Simeon fault zone, south-central coastal California: in Alterman, I., McMullen, R.B., Cluff, L.S.,

and Slemmons, D.B. (editors), *Seismotectonics of the Central California Coast Ranges*, Geological Society of America Special Paper 292, pp. 133–150.

Hanson, K.L., Lettis, W.R., McLaren, M.K., Savage, W.U., and Hall, N.T., 2004. Style and rate of Quaternary deformation of the Hosgri fault zone, offshore south-central California: in Keller, M.A. (editor), *Evolution of Sedimentary Basins/Onshore Oil and Gas Investigations—Santa Maria Province*, U.S. Geological Survey Bulletin 1995-BB, 33 pp.

Hardebeck, J.L., 2010. Seismotectonics and fault structure of the California central coast, *Bulletin of the Seismological Society of America* **100** (3): 1031–1050.

Hardebeck, J.L., 2012. Seismicity of the Shoreline and Hosgri Faults, Estero Bay and Irish Hills, PowerPoint presentation at DCPD SSHAC Workshop #2, 6 November.

Hardebeck, J.L., 2013. Geometry and earthquake potential of the Shoreline fault, central California, *Bulletin of the Seismological Society of America* **103** (1): 447–462.

Hardebeck, J.L., 2014. Seismicity and Fault Structures of Estero Bay and the Irish Hills, PowerPoint presentation at DCPD SSHAC Workshop #3, 26 March.

Hardebeck, J.L., and P.M. Shearer (2002). A new method for determining first-motion focal mechanisms, *Bull. Seismol. Soc. Am.* **92**, 2264–2276.

High Energy Seismic Survey Team, 1999. *High Energy Seismic Survey Review Process and Interim Operational Guidelines for Marine Surveys Offshore Southern California*, California State Lands Commission and U.S. Mineral Management Service, 98 pp.

Honjas, W., Louie, J.N., and Pullammanappallil, S.K., 1995. Cenozoic tectonic history of the Hosgri Fault Zone, offshore California from seismic imaging and stratigraphic analysis, unpublished report, available at <http://crack.seismo.unr.edu/ftp/pub/louie/papers/hosgri/PAPER.html>

Hoskins, E.G., and Griffiths, R.R., 1971. Hydrocarbon potential of northern and central California offshore in Cram, I.H. (editor), *Future Petroleum Provinces of the United States—Their Geology and Potential*, American Association of Petroleum Geologists Memoir 15, pp. 212–222.

Howie, J.M., Miller, K.C., and Savage, W.U., 1993. Integrated crustal structure across the south central California margin: Santa Lucia escarpment to the San Andreas Fault, *Journal of Geophysical Research* **98**: 8173–8196.

Independent Peer Review Panel, IPRP, 2012a. Comments on PG&E's Enhanced Seismic Study Progress Presentation for Diablo Canyon Power Plant, Report No 3, 6 April.

Independent Peer Review Panel, IPRP, 2012b. Comments on PG&E's Enhanced Seismic Study Progress Presentation for Diablo Canyon Power Plant, Report No. 4, 25 September.

Jachens, R.C., Wentworth, C.M., and McLaughlin, R.J., 1998. Pre-San Andreas location of the Gualala block inferred from magnetic and gravity anomalies: in Elder, W.P. (editor), *Geology and Tectonics of the Gualala Block, Northern California*, Pacific Section, Society of Economic Paleontologists and Mineralogists, Book, 84, pp. 27–64.

Johnson, S.Y., and Watt, J.T., 2012. Influence of fault trends, bends, and convergence on shallow structure and geomorphology of the Hosgri strike-slip fault, offshore central California, *Geosphere* **8**: 1–25.

Kame, N., Rice, J.R., and Dmowska, R., 2003. Effects of prestress state and rupture velocity on dynamic fault branching, *Journal of Geophysical Research* **108**: ESE13-1–ESE 13-21.

Klein, F.W., 1989. *Users Guide to HYPOINVERSE, a Program for VAX Computers to Solve for Earthquake Location and Magnitudes*, U.S. Geological Survey Open-File Report 89-314.

Lafond, C.F., and Levander, A.R., 1993. Migration moveout analysis and depth focusing, *Geophysics* **58** (1): 91–100.

Langenheim, V.E., 2013. *Gravity, Aeromagnetic and Rock-Property Data of the Central California Coast Ranges*, U.S. Geological Survey Open-File Report 2013-1282, 12 pp.

Langenheim, V.E., Jachens, R.C., Graymer, R.W., Colgan, J.P., Wentworth, C.M., and Stanley, R.G., 2013. Fault geometry and cumulative offsets in the Central Coast Ranges, California: Evidence for northward increasing slip along the San Gregorio–San Simeon–Hosgri fault, *Lithosphere* **5** (1): 29–48

Langenheim, V.E., Jachens, R.C., and Moussaoui, K., 2009. *Aeromagnetic Survey Map of the Central California Coast Ranges*, U.S. Geological Survey Open-File Report 2009-1044.

Langenheim, V.E., Watt, J.T., and Denton, K.D., 2012. Magnetic map of the Irish Hills and surrounding area, central California, U.S. Geological Survey Open-File Report 2012-1080, scale 1:24,000.

Leslie, R.B., 1981. *Continuity and Tectonic Implications of the San Simeon-Hosgri Fault Zone, Central California*, U.S. Geological Survey Open-File Report 81-430, 59 pp.

Lettis, W.R., Hanson, K.L., Unruh, J.R., McLaren, M., and Savage, W.U., 2004. Quaternary tectonic setting of south-central coastal California: in Keller, M.A. (editor), *Evolution of Sedimentary Basins/Offshore Oil and Gas Investigations—Santa Maria Province*, U.S. Geological Survey Bulletin 1995-AA, 24 pp.

Lettis, W.R., DiSilvestro, L., Hanson, K.L., and Shiller, G.I., 1990. The San Simeon/Hosgri pull-apart basin: Implications for late Quaternary activity on the Hosgri Fault Zone: in Lettis, W.R., Hanson, K.L., Kelson, K.I., and Wesling, J.R. (editors),

*Neotectonics of the South-Central Coastal California*, Friends of the Pleistocene, Pacific Cell, 1990 Fall Field Trip Guidebook, pp. 91–138.

Lindh, A., Motooka, C., Ball, S., and Dollar, R., 1981. *Current Seismicity of the Central California Coastal Region from Point Buchon to Point Piedras Blancas: A Preliminary Report*, U.S. Geological Survey Open-File Report 81-44, 16 pp.

McCulloch, D.S., and Chapman, R.H., 1977. *Maps Showing Residual Magnetic Intensity Along the California Coast, Lat. 37 Degrees 30' N to Lat. 34 Degrees 30' N*, U.S. Geological Survey Open-File Report 77-79, 14 aeromagnetic maps, scale 1:250,000.

McIntosh, K.D., Reed, D.L., Silver, E.A., and Meltzer, A.S., 1991. Deep structure and structural inversion along the central California continental margin from EDGE seismic profile RU-3, *Journal of Geophysical Research* **96**: 6459–6473.

McLaren, M.K., and Savage, W.U., 2001. Seismicity of south-central coastal California: October 1987 through January 1997, *Bulletin of the Seismological Society of America* **91** (6): 1629–1658.

Meltzer, A.S., and Levander, A.R., 1991. Deep crustal reflection profiling offshore southern central California, *Journal of Geophysical Research* **96** (B4): 6475–6491.

Miller, K.C., and Meltzer, A.S., 1999. Structure and tectonics of the central offshore Santa Maria and Santa Lucia basins, California- Results from the PG&E EDGE seismic reflection survey: in Keller, M.A. (editor), *Evolution of Sedimentary Basins/Onshore Oil and Gas Investigations—Santa Maria Province*, U.S. Geological Survey Bulletin 1995-Z, 12 pp.

Namson, J.S., and Davis, T.L., 1990. Late Cenozoic fold and thrust belt of the southern Coast Ranges and Santa Maria basin, California, *American Association of Petroleum Geologists Bulletin* **74**: 467–492.

Ouillon, G., Ducorbier, C., and Sornette, D., 2008. Automatic reconstruction of fault networks from seismicity catalogs: Three-dimensional optimal anisotropic dynamic clustering, *Journal of Geophysical Research* **113**, 15 pp.

Pacific Gas and Electric Company (PG&E), 1988a. *Final Report of the Diablo Canyon Long-Term Seismic Program*, U.S. Nuclear Regulatory Commission Docket Nos. 50-275 and 50-323.

Pacific Gas and Electric Company (PG&E), 1988b. LTSP Plate Q43m-2, U.S. Nuclear Regulatory Commission Docket Nos. 50-275 and 50-323.

Pacific Gas and Electric Company (PG&E), 1990. *Response to Nuclear Regulatory Commission Questions GSG-12 and GSG-16 on the Final Report of the Diablo Canyon Long-Term Seismic Program*, U.S. Nuclear Regulatory Commission Docket Nos. 50-275 and 50-323.

Pacific Gas and Electric Company (PG&E), 2011. *Report on the Analysis of the Shoreline Fault Zone, Central Coastal California*, U.S. Nuclear Regulatory Commission Docket Nos. 50-275 and 50-323.

Pacific Gas and Electric Company (PG&E), 2014 *DCPP 3D/2D Seismic-Reflection Investigation of Structures Associated with the Northern Shoreline Seismicity Sublineament of the Point Buchon Region*, Technical Report GEO.DCPP.TR.12.01, Rev.1.

Pullammanappallil, S.K., and Louie, J.N., 1994. A generalized simulated-annealing optimization for inversion of first arrival times, *Bulletin of the Seismological Society of America* **84** (5): 1397–1409.

Reasenber, P.A., and D. Oppenheimer (1985). FPFIT, FPLOT, and FPPAGE: Fortran computer programs for calculating and displaying earthquake fault-plane solutions, *U.S. Geol. Surv. Open-File Rept.* 85–739.

Roecker, S.W., 1981. Seismicity and Tectonics of the Pamir-Hindu Kush Region of Central Asia, Ph.D. thesis, Massachusetts Institute of Technology.

Sedlock, R.L., and Hamilton, D.H., 1991. Late Cenozoic tectonic evolution of southwestern California, *Journal of Geophysical Research* **96**: 2325–2351.

Shih, R.C., and Levander, A.R., 1994. Layer-stripping reverse-time migration, *Geophysical Prospecting* **41**: 211–227.

Silver, E.A., and Normark, W.R. (editors), 1978. *San Gregorio–Hosgri Fault Zone, California*, California Division of Mines and Geology Special Report 137, 56 pp.

Sliter, R.W., Triezenberg, P.J., Hart, P.E., Watt, J.T., Johnson, S.Y., and Scheirer, D.S., 2009. *High-Resolution Seismic-Reflection and Marine Magnetic Data Along the Hosgri Fault Zone, Central California*, U.S. Geological Survey Open File Report 2009-1100, version 1.1

Sorlien, C.C., Kamerling, M.J., and Mayerson, D., 1999. Block rotation and termination of the Hosgri strike slip fault, California, from three-dimensional map restoration, *Geology* **27** (11): 1039–1042.

Steritz, J.W., and Luyendyk, B.P., 1994. Hosgri fault zone, offshore Santa Maria Basin, California: in Alterman, I.B., McMullen, R.B., Cluff, L.S., and Slemmons, D.B. (editors), *Seismotectonics of the Central California Coast Ranges*, Geological Society of America Special Paper 292, pp. 191–209.

Trehu, A., 1991. Tracing the subducted oceanic crust beneath the central California continental margin: Results from ocean bottom seismometers deployed during the 1986 Pacific Gas and Electric EDGE experiment, *Journal of Geophysical Research* **96**: 6493–6506.

Underwood, M.B., and Laughland, M.B., 2001. Paleothermal structure of the Point San Luis slab of central California: Effects of Late Cretaceous underplating, out-of-sequence thrusting, and late Cretaceous dextral offset, *Tectonics* **20**: 97–111.

Wagner, H.C., 1974. *Marine Geology Between Cape San Martin and Point Sal, South-Central California Offshore*, U.S. Geological Survey Open-File Report 74-252, 17 pp.

Waldhauser, F., and Ellsworth, W.L., 2000. A double-difference earthquake location algorithm: method and application to the northern Hayward Fault, California, *Bulletin of the Seismological Society of America* **90**: 1353–1368.

Watt, J.T., 2012. Gravity and Magnetic Constraints for the Hosgri and Shoreline Faults, PowerPoint presentation at DCPD SSHAC Workshop #2, 6 November.

Watt, J.T., Johnson, S.Y., and Langenheim, V.E., 2011. Fault intersections along the Hosgri Fault Zone, central California, *Transactions of the American Geophysical Union* abstract GP41A-0977.

Weber, G.E., 1994. Late Pleistocene slip rates on the San Gregorio Fault Zone at Point Año Nuevo, San Mateo County, California: in Lettis, W.R. (editor), *Field Trip Guidebook to Transpressional Deformation in the San Francisco Bay Region*, Friends of the Pleistocene, Pacific Southwest Cell.

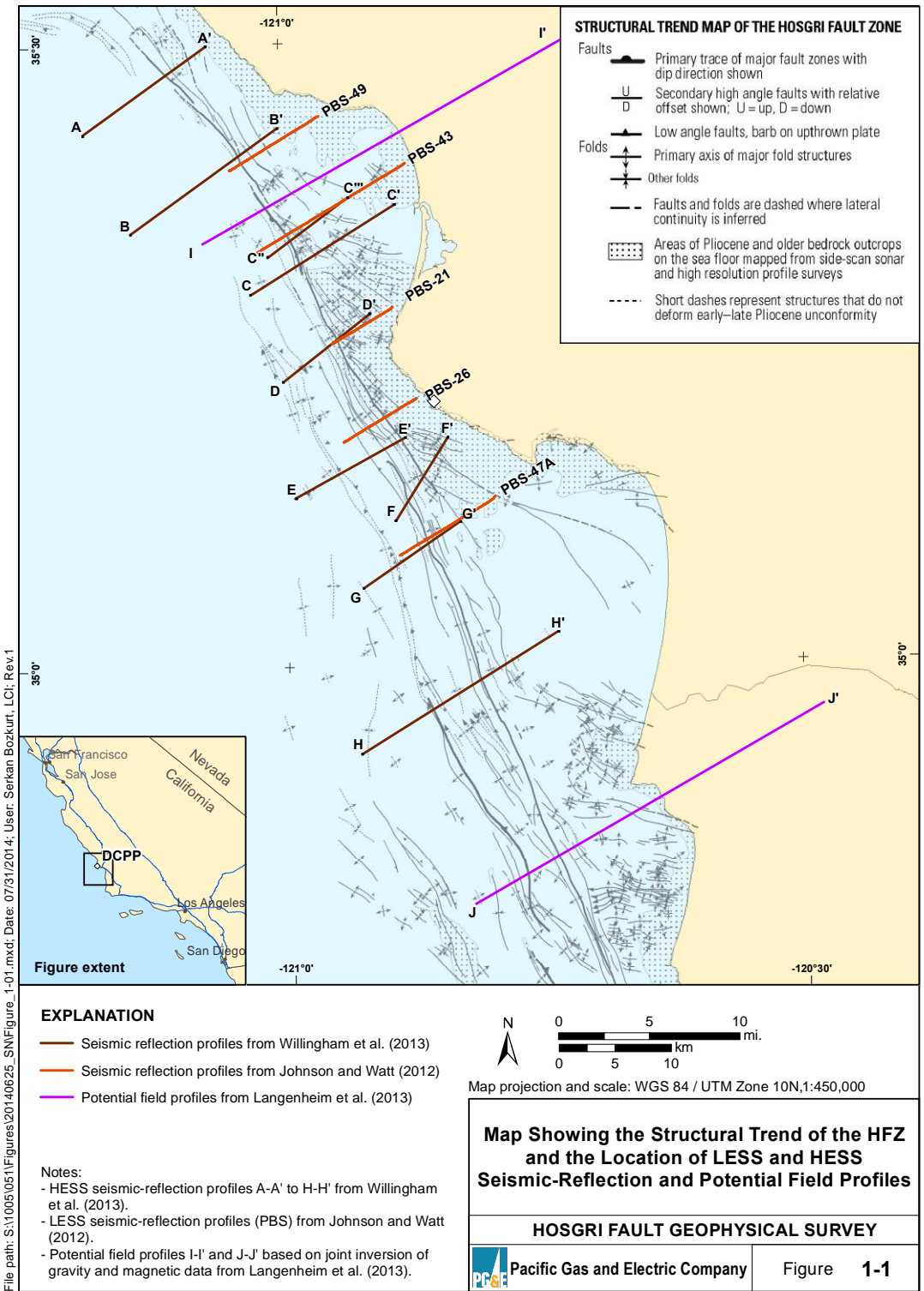
Wesnousky, S.G., 2006. Predicting the endpoints of earthquake ruptures, *Nature* **444**: 358–360.

Willingham, C.R., Rietman, J.D., Heck, R.G., and Lettis, W.R., 2013. Characterization of the Hosgri Fault Zone and adjacent structures in the offshore Santa Maria Basin, south-central California: in Keller, M.A. (editor), *Evolution of Sedimentary Basins/Onshore Oil and Gas Investigations—Santa Maria Province*, U.S. Geological Survey Bulletin 1995-CC, 105 pp.

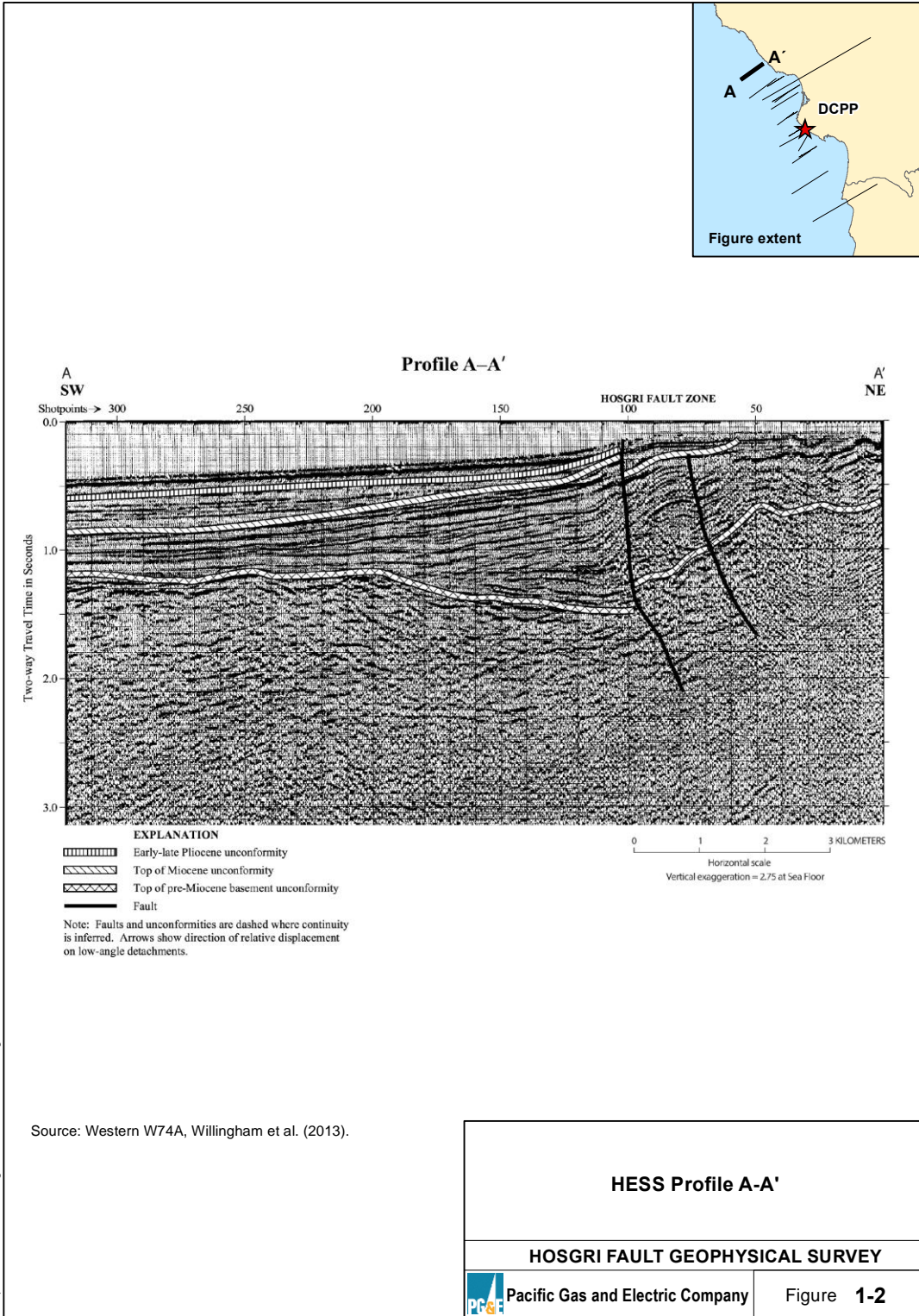
Worden, C.B., 1992. Interactive Seismic Imaging on a Multicomputer and Application to the Hosgri Fault, Ph.D. dissertation, California Institute of Technology.

Zhang, H., and Thurber, C.H., 2003. Double-difference tomography: The method and its application to the Hayward fault, California, *Bulletin of the Seismological Society of America* **93**: 1875–1889.



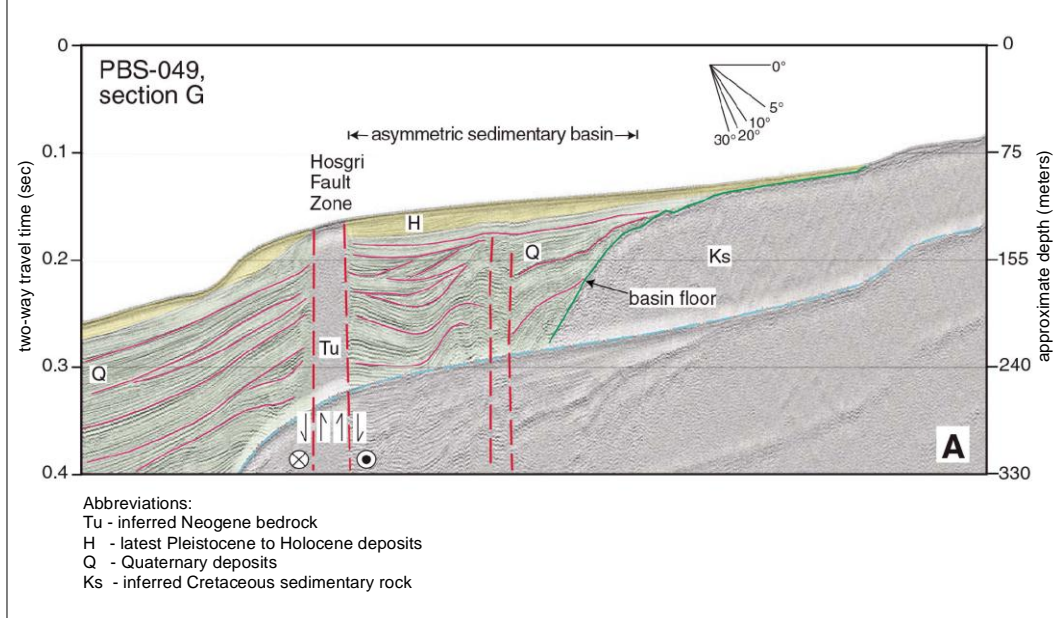


File path: S:\1005\051\Figures\20140625\_SN\Figure\_1-01.mxd; Date: 07/31/2014; User: Serkan Bozkurt, LCI; Rev: 1

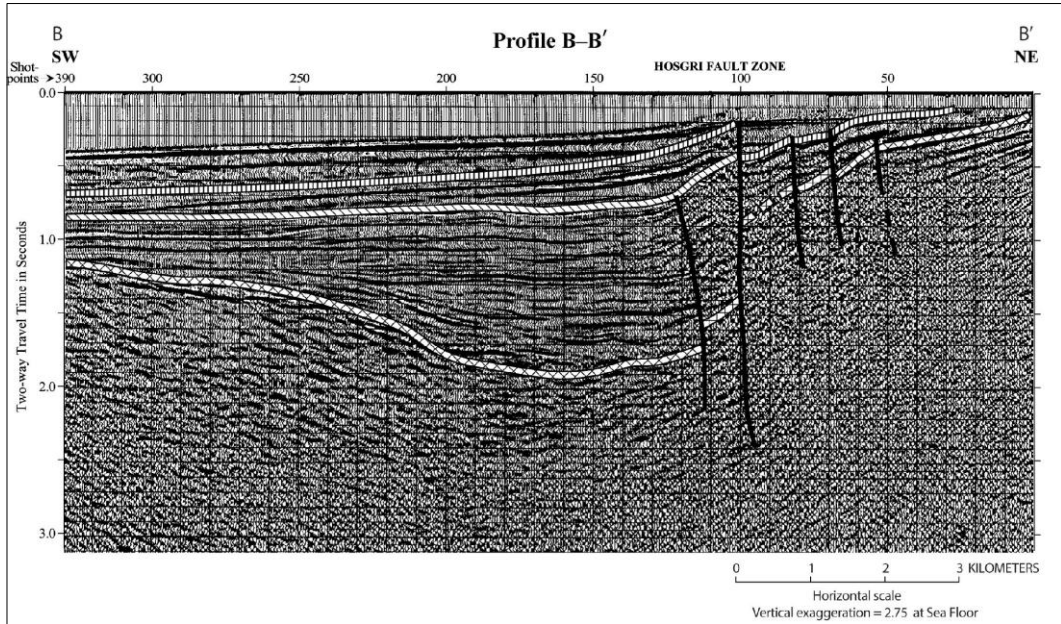


File path: S:\1005\051\Figures\20140625\_SNI\Figure\_1-02.mxd; Date: 07/31/2014; User: Serkan Bozkurt, LC; Rev: 1

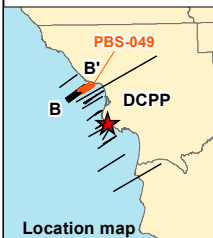
(a) USGS 2D LESS profile (PBS-049, Johnson and Watt, 2012)



(b) HESS Profile B - B' (Western W76A, Willingham et al., 2013)



File path: S:\10051051\Figures\20140625\_SNI\Figure\_1-03.mxd; Date: 07/31/2014; User: Alex Remar, LCI; Rev.1



**EXPLANATION**

- Early-late Pliocene unconformity
  - Top of Miocene unconformity
  - Top of pre-Miocene basement unconformity
  - Fault
- Note: Faults and unconformities are dashed where continuity is inferred. Arrows show direction of relative displacement on low-angle detachments.

Note: Difference in vertical scale exists between (a) and (b).

**USGS 2D LESS Profile PBS-049 and HESS Profile B - B'**

**HOSGRI FAULT GEOPHYSICAL SURVEY**

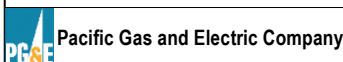
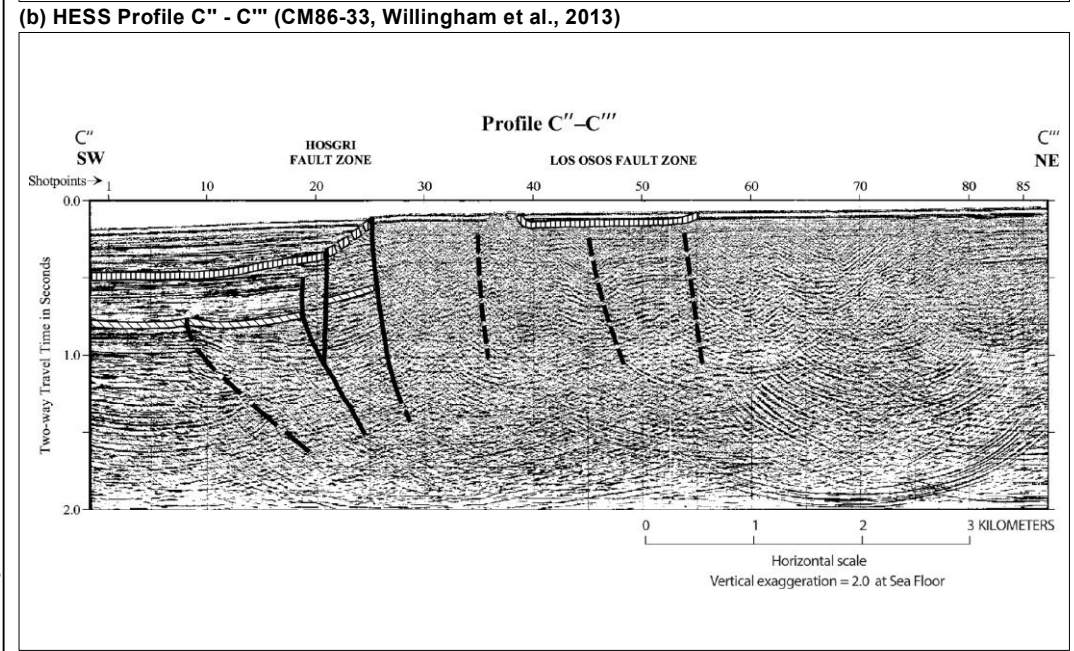
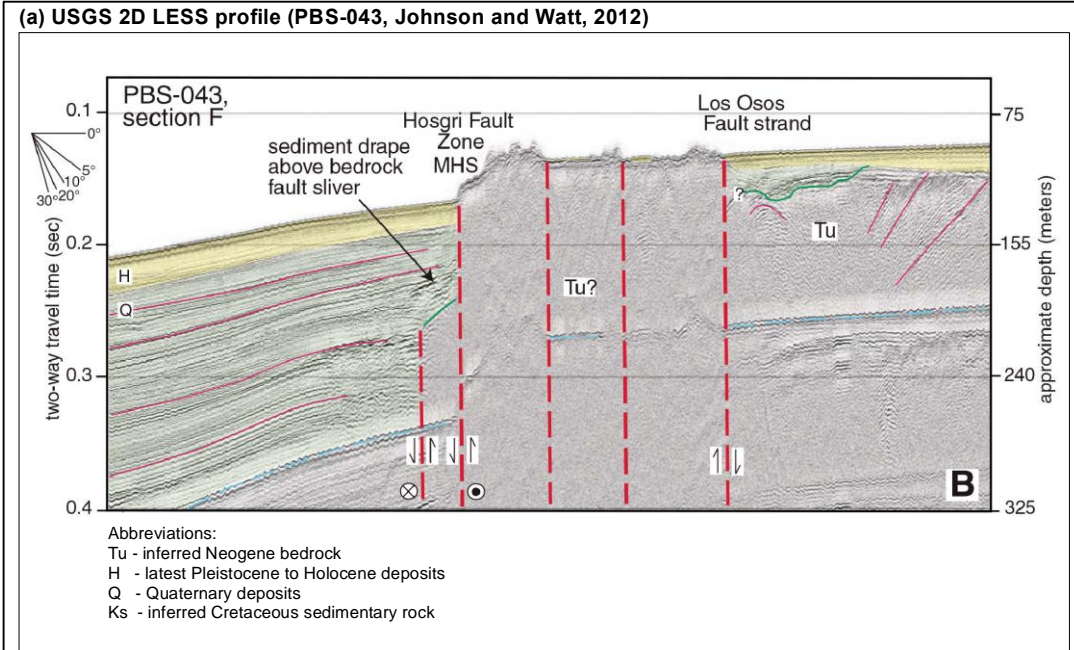
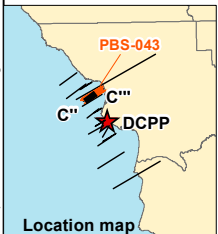


Figure 1-3



File path: S:\1005\051\Figures\20140625\_SNI\Figure\_1-04.mxd; Date: 07/31/2014; User: Alex Remar; LCI: Rev.1



**EXPLANATION**

- Early-late Pliocene unconformity
- Top of Miocene unconformity
- Top of pre-Miocene basement unconformity
- Fault

Note: Faults and unconformities are dashed where continuity is inferred. Arrows show direction of relative displacement on low-angle detachments.

Note: Difference in vertical scale exists between (a) and (b).

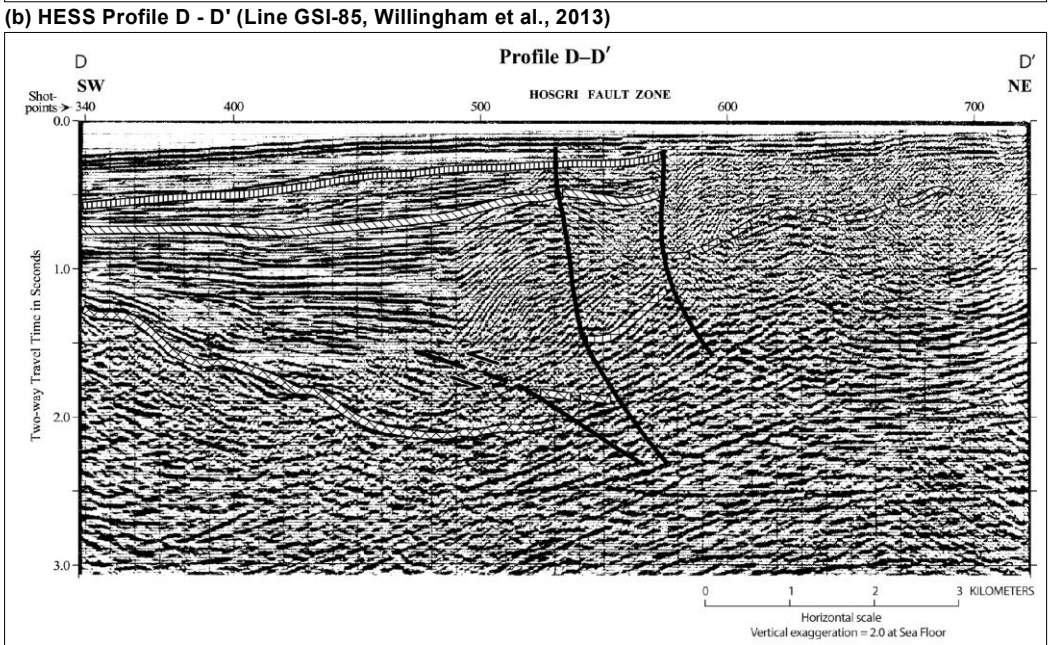
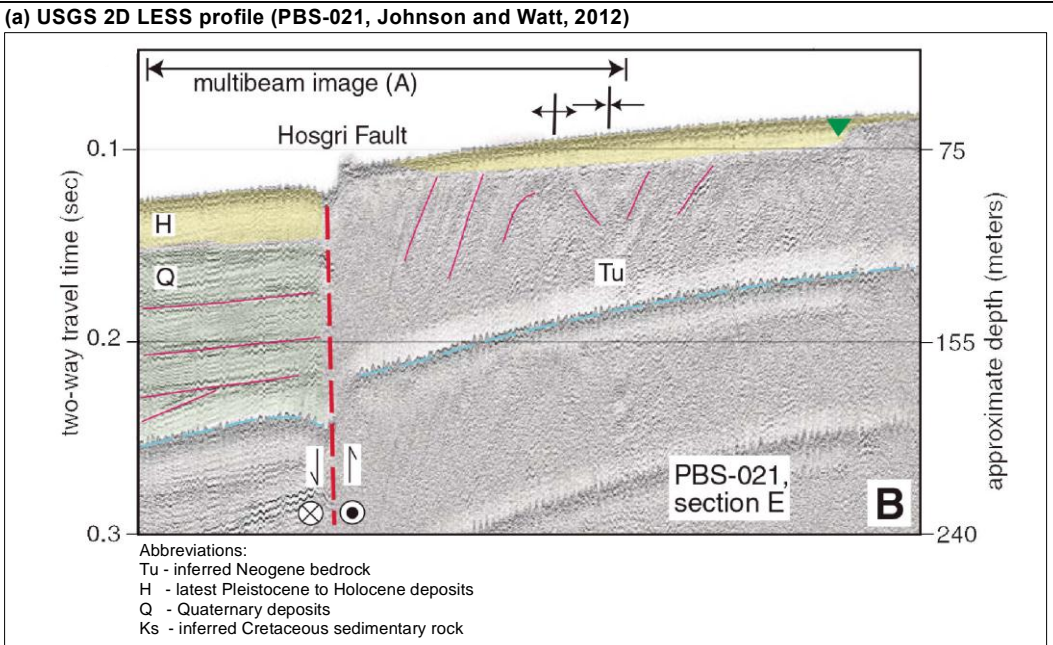
**USGS 2D LESS Profile PBS-043  
 and HESS Profile C'' - C'''**

---

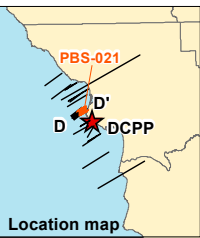
**HOSGRI FAULT GEOPHYSICAL SURVEY**

---

Pacific Gas and Electric Company
 Figure **1-4**



File path: S:\1005\051\Figures\20140625\_SNI\Figure\_1-05.mxd; Date: 07/31/2014; User: Alex Remar, LCI; Rev: 1



**EXPLANATION**

- Early-late Pliocene unconformity
- Top of Miocene unconformity
- Top of pre-Miocene basement unconformity
- Fault

Note: Faults and unconformities are dashed where continuity is inferred. Arrows show direction of relative displacement on low-angle detachments.

Note: Difference in vertical scale exists between (a) and (b).

**USGS 2D LESS Profile PBS-021  
 and HESS Profile D - D'**

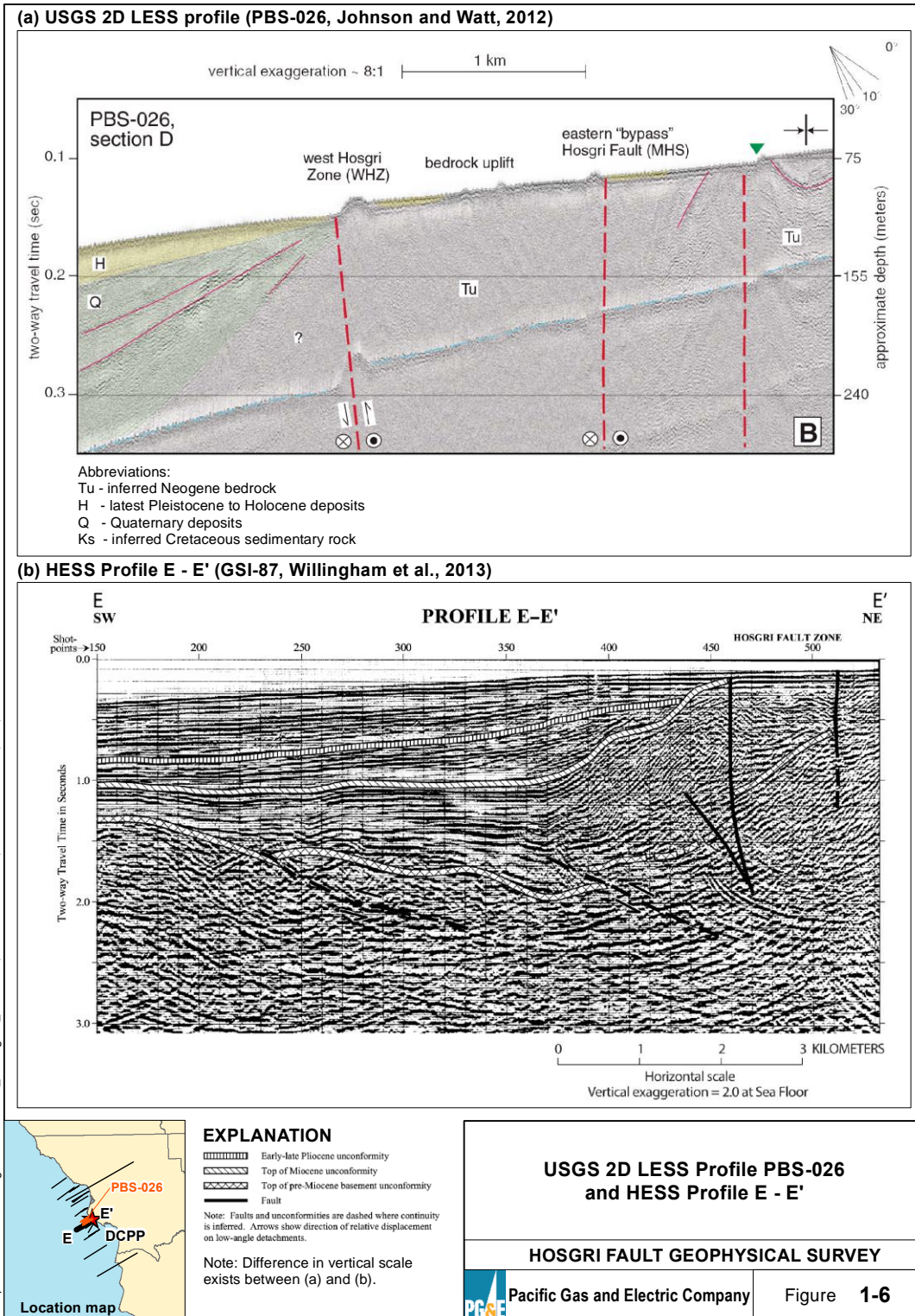
---

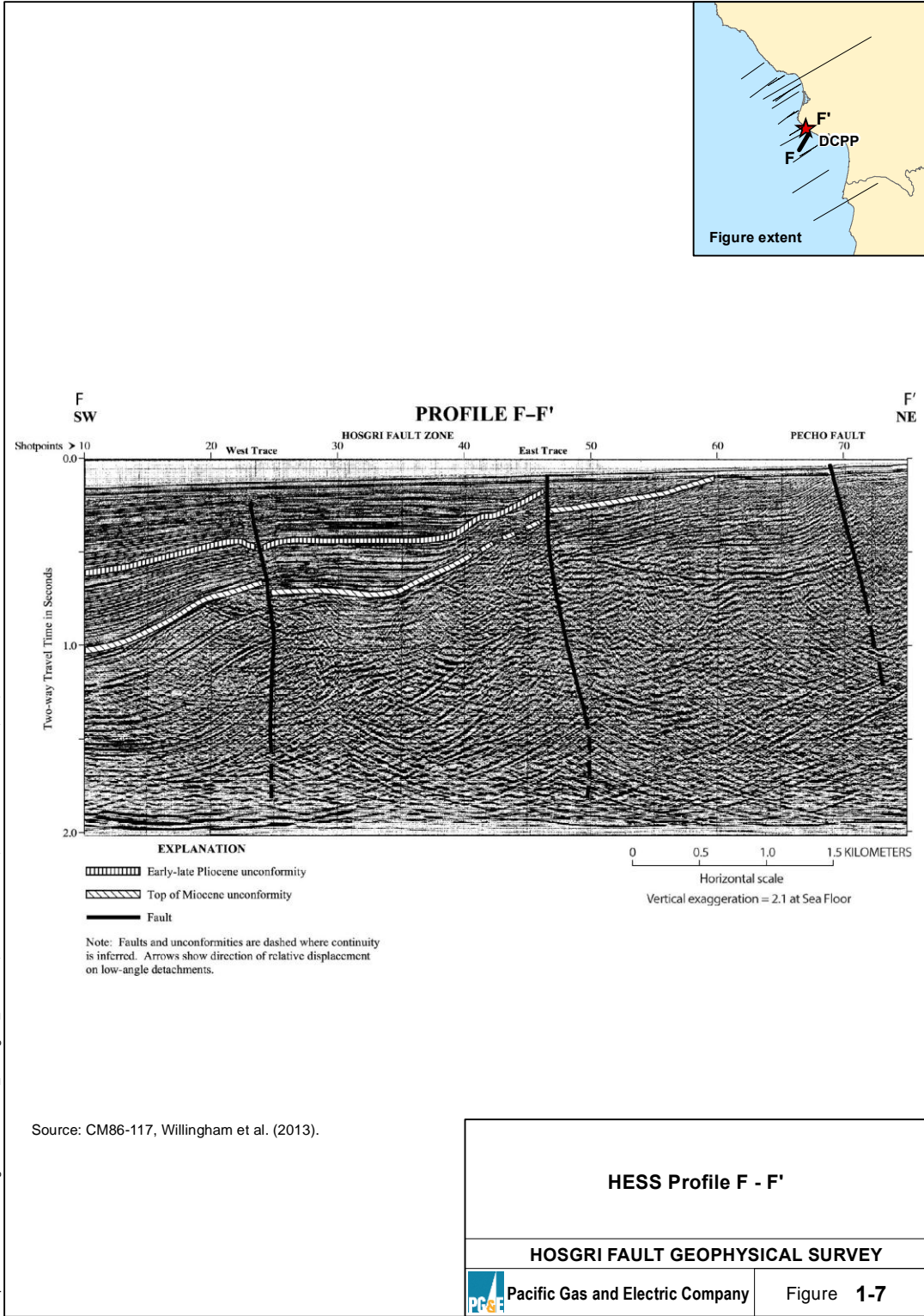
**HOSGRI FAULT GEOPHYSICAL SURVEY**

---

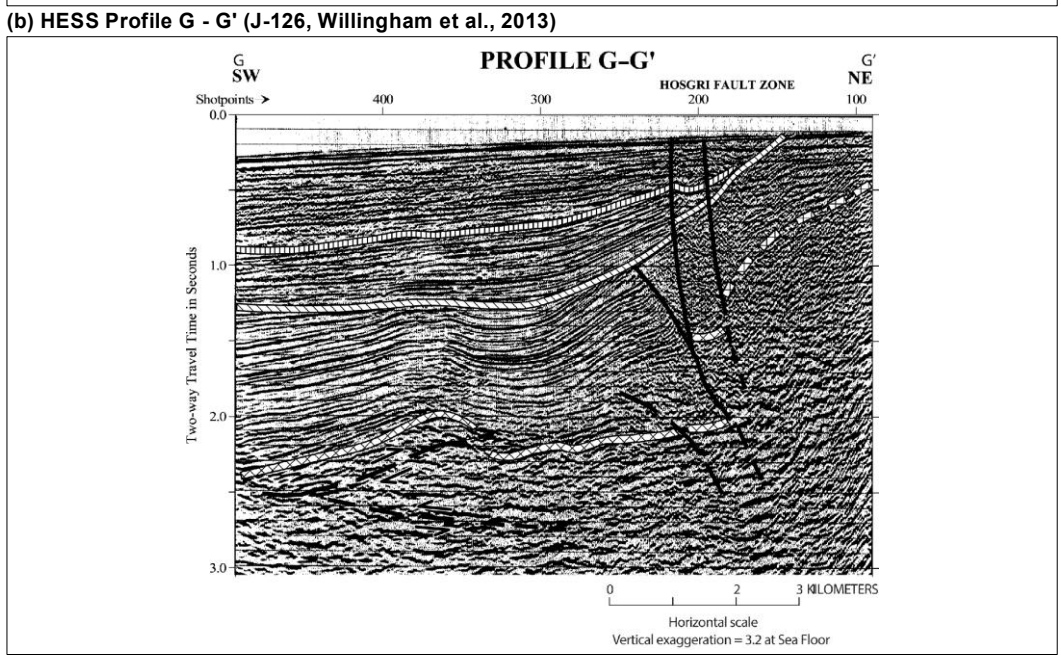
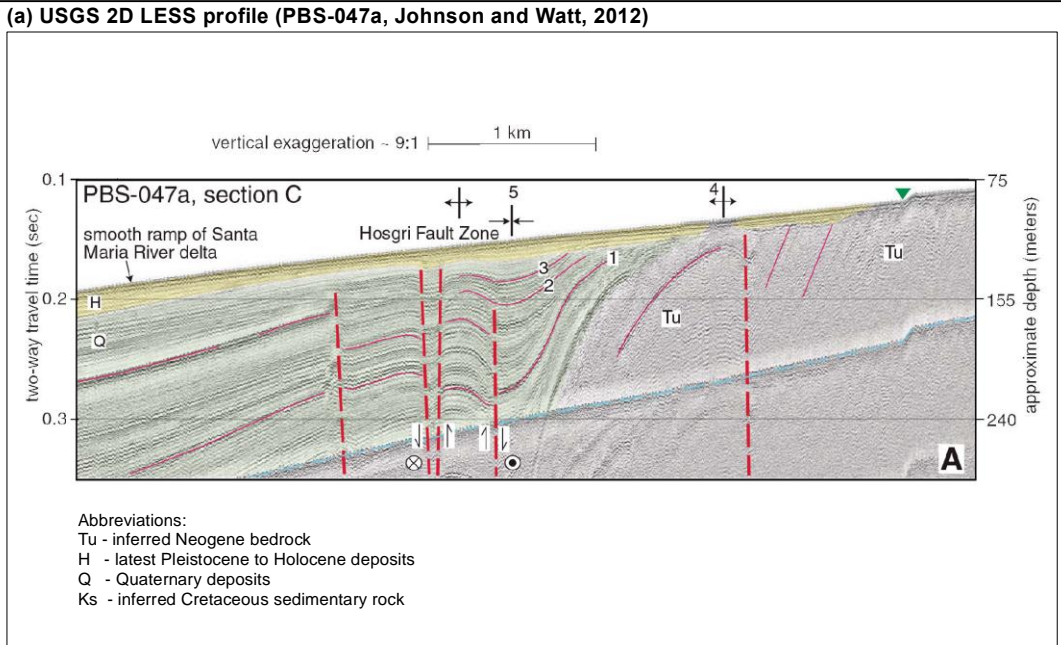
Pacific Gas and Electric Company

Figure **1-5**

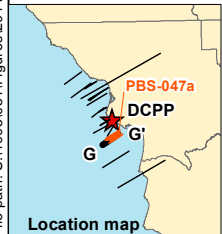




File path: S:\1005\051\Figures\20140625\_SNI\Figure\_1-07.mxd; Date: 07/31/2014; User: Serkan Bozkurt, LC; Rev: 1



File path: S:\1005051\Figures\20140625\_SNI\Figure\_1-08.mxd; Date: 07/31/2014; User: Alex Remar, LC; Rev: 1



**EXPLANATION**

- Early-late Pliocene unconformity
- Top of Miocene unconformity
- Top of pre-Miocene basement unconformity
- Fault

Note: Faults and unconformities are dashed where continuity is inferred. Arrows show direction of relative displacement on low-angle detachments.

Note: Difference in vertical scale exists between (a) and (b).

**USGS 2D LESS Profile PBS-047a  
 and HESS Profile G - G'**

---

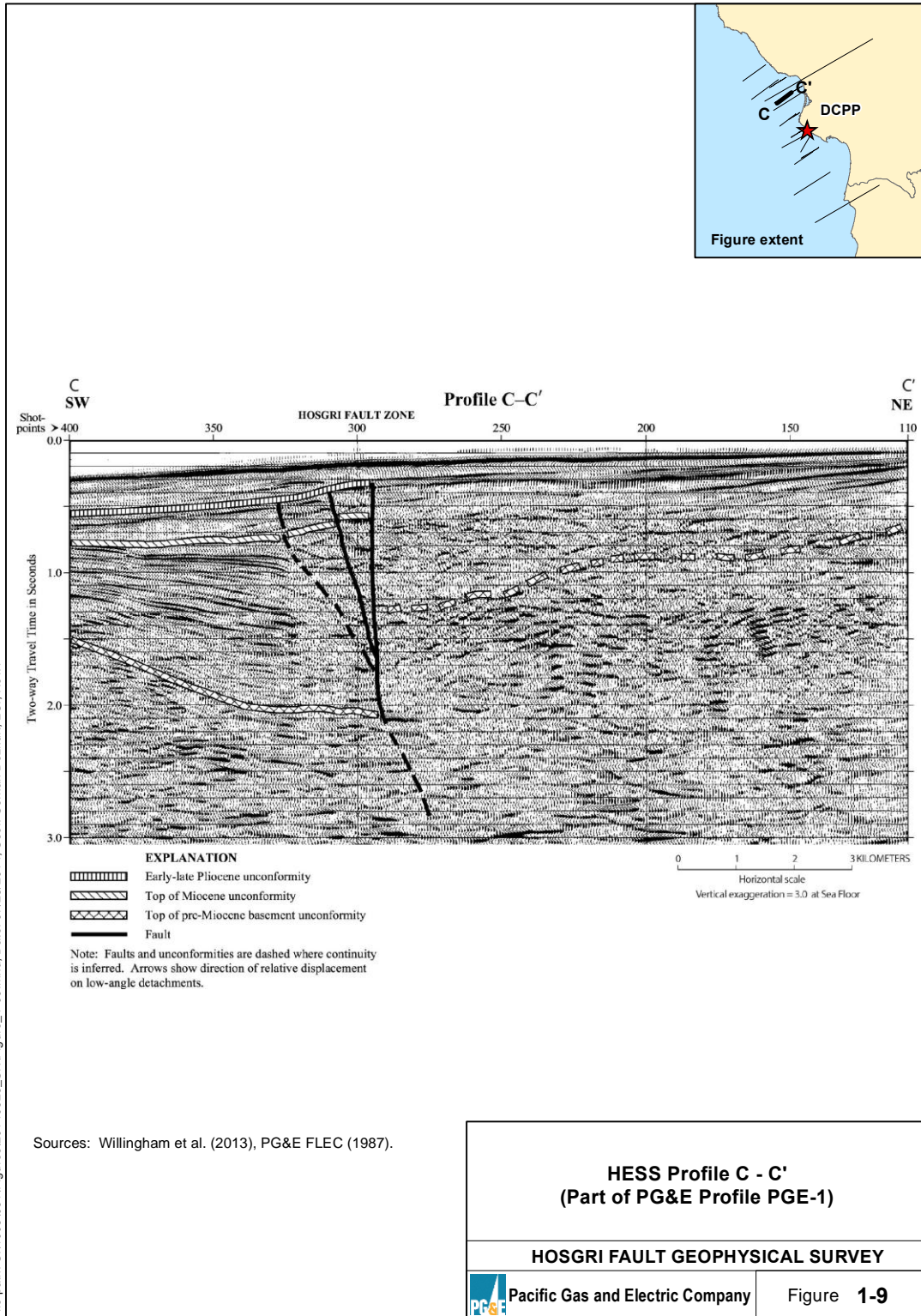
**HOSGRI FAULT GEOPHYSICAL SURVEY**

---

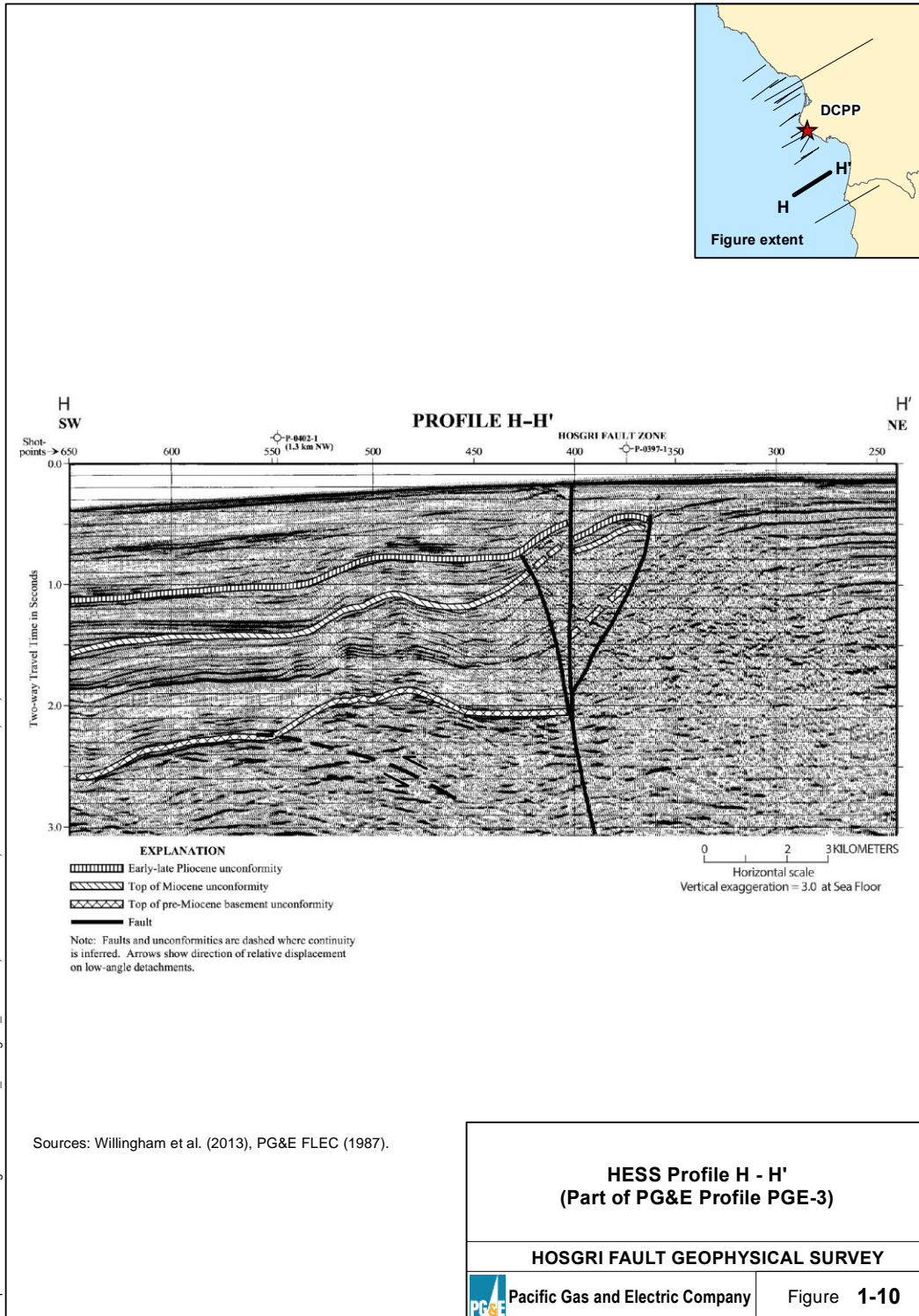
Pacific Gas and Electric Company

Figure 1-8



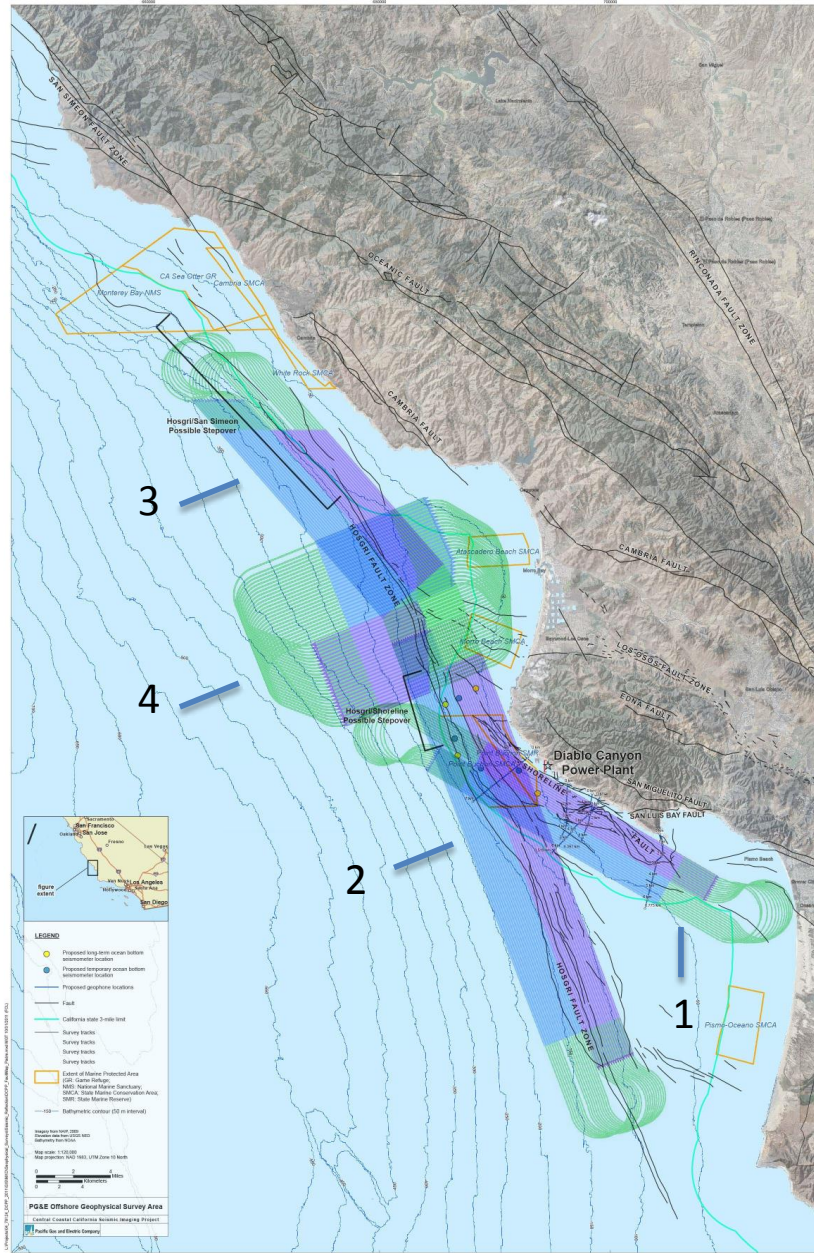


File path: S:\1005\05\Figures\20140625\_SNI\Figure\_1-09.mxd, Date: 07/28/2014, User: Serkan Bozkurt, LCI, Rev.1

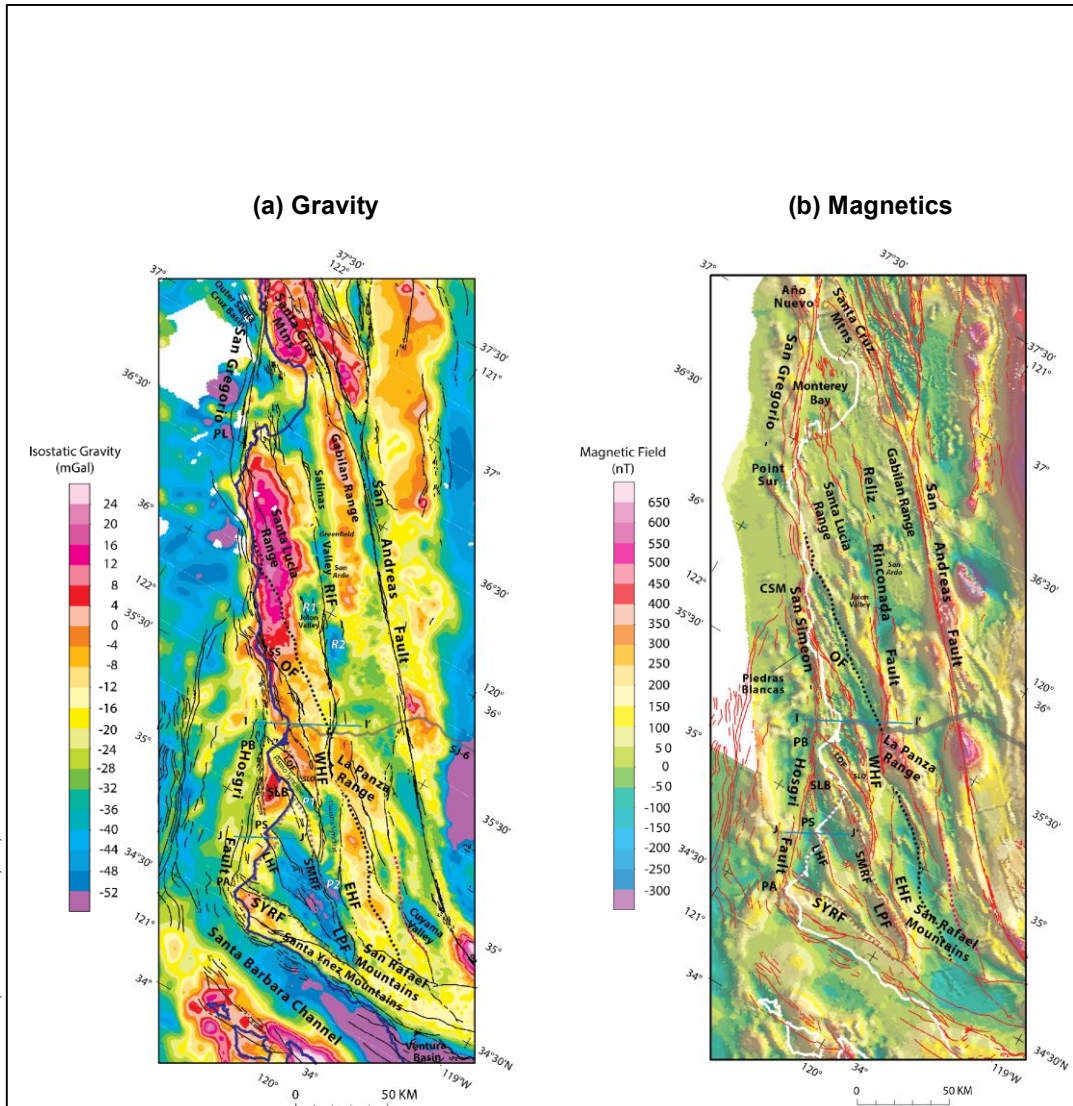


File path: S:\1005\051\Figures\20140625\_SNI\Figure\_1-10.mxd; Date: 07/28/2014; User: Serkan Bozkurt, LCI; Rev.1

S:\1005051\Figures\20140625\_SNI\Figure\_1-11.ai; Date: 07/17/2014; User: Serkan Bozkurt, LC; Rev: 1

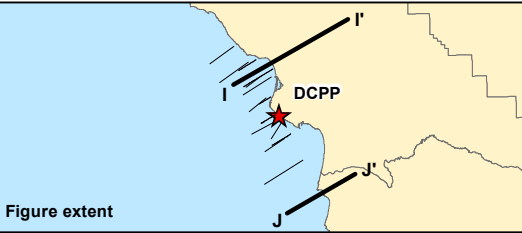



<b>Proposed Track Lines for PG&amp;E CCCSIP HESS.</b>	
<b>PROJECT TITLE</b>	
Pacific Gas and Electric Company	Figure <b>1-11</b>

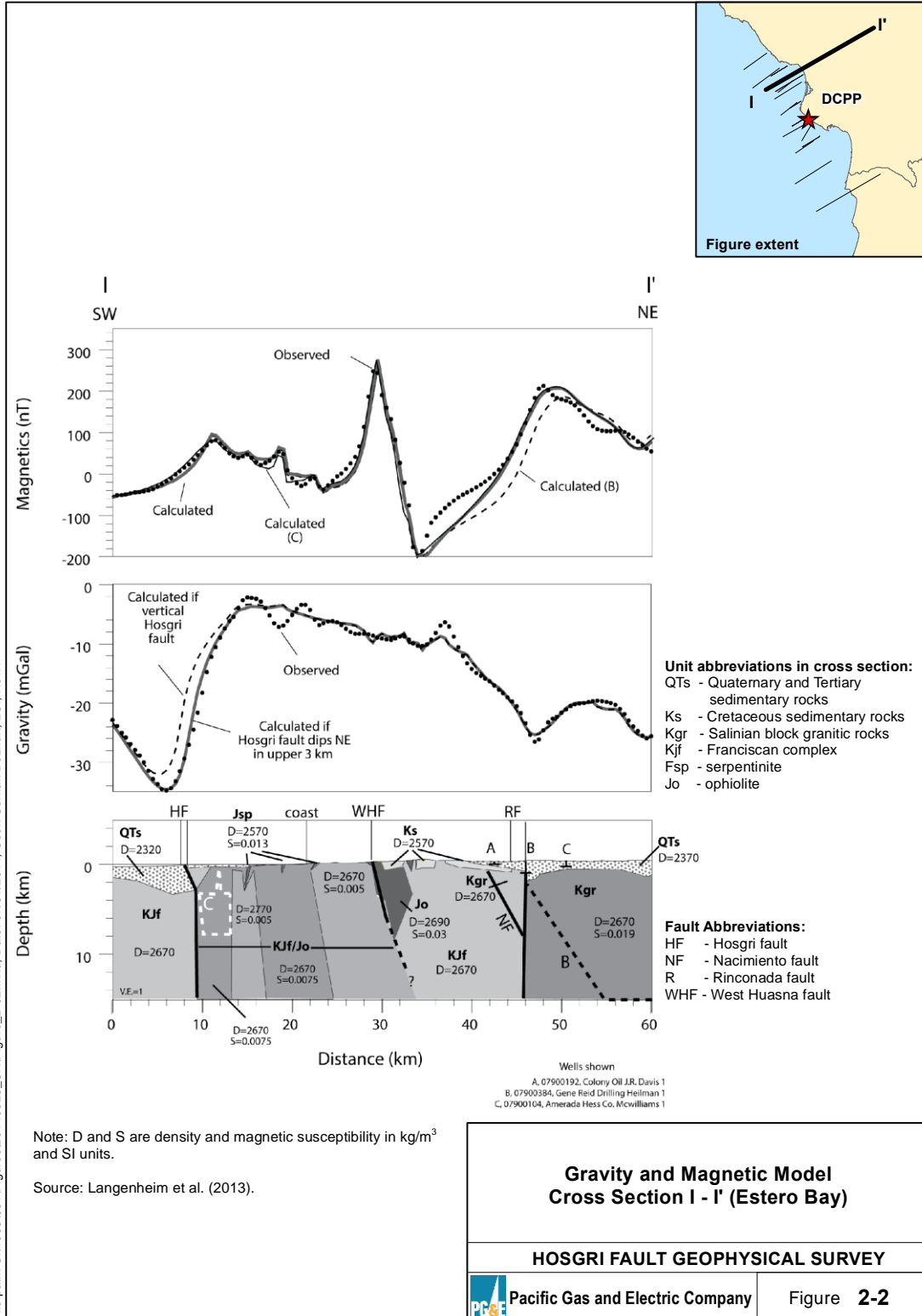


- Abbreviations:**
- |                         |                               |                    |                       |
|-------------------------|-------------------------------|--------------------|-----------------------|
| LHF - Lions Head fault  | SYRF - Santa Ynez River fault | PB - Point Buchon  | SLO - San Luis Obispo |
| LOF - Los Osos fault    | WHF - West Huasna fault       | PL - Point Lobos   | SS - San Simeon       |
| LPF - Little Pine fault | CSM - Cape San Marin          | PS - Point Sal     |                       |
| OF - Oceanic fault      | PA - Point Arguello           | SLB - San Luis Bay |                       |

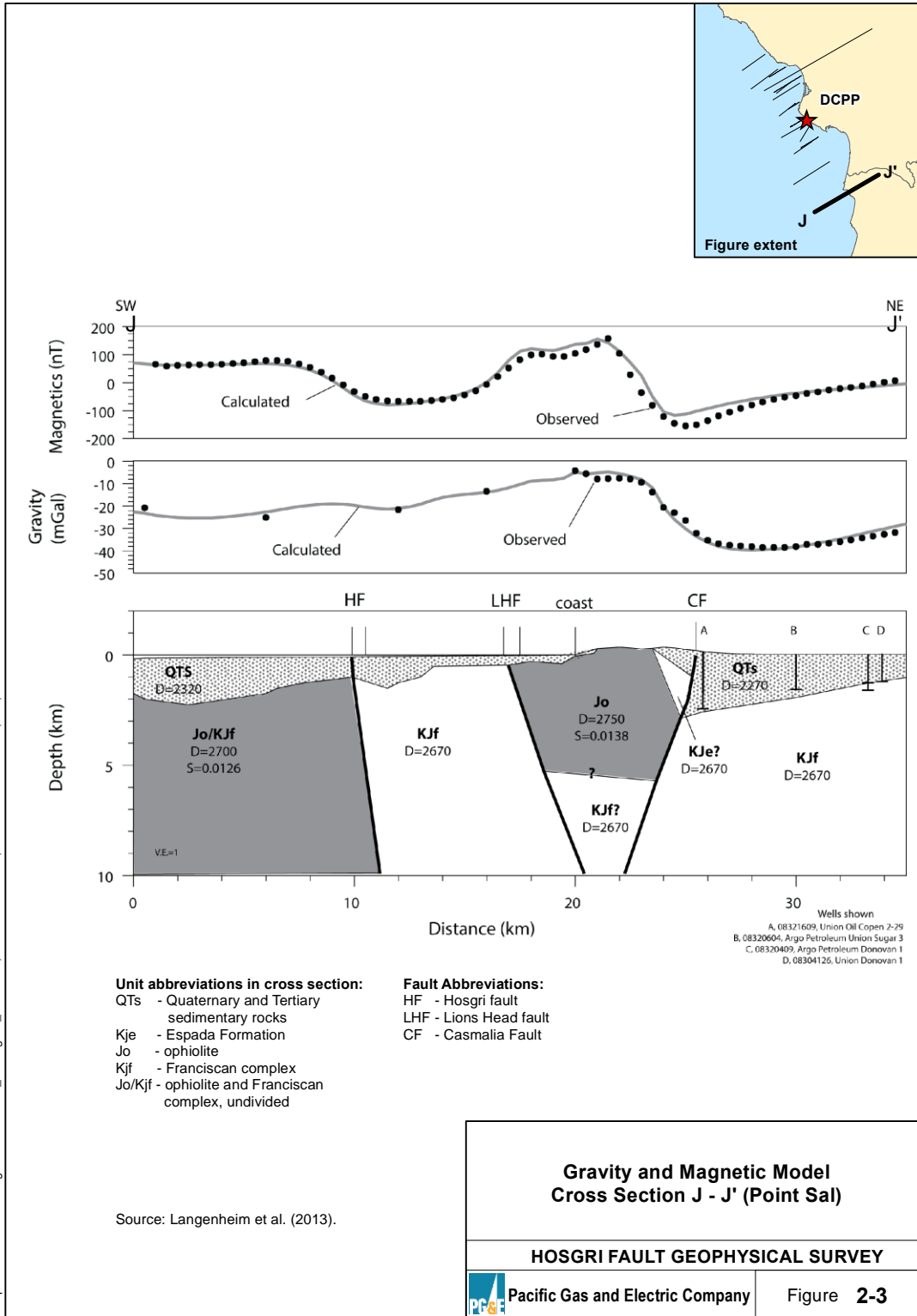
Source: Langenheim et al. (2013).

 <p>Figure extent</p>	<p><b>Potential Field Maps for California Coastal Region</b></p> <hr/> <p><b>HOSGRI FAULT GEOPHYSICAL SURVEY</b></p> <hr/> <p> Pacific Gas and Electric Company</p>
<p>Figure 2-1</p>	

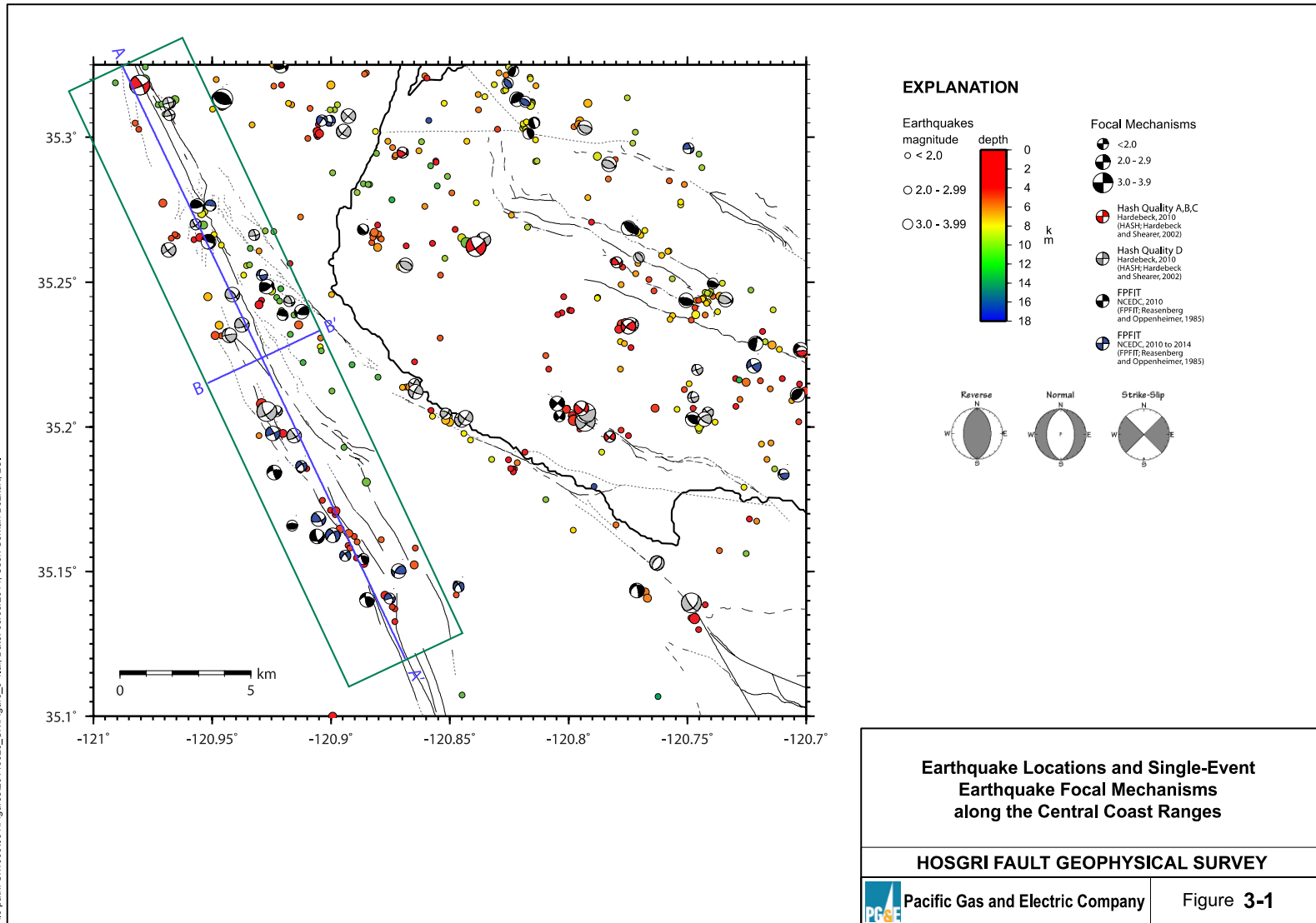
File path: S:\1005\051\Figures\20140625\_SNI\Figure\_2-01.mxd; Date: 07/31/2014; User: Alex Remar, LCI; Rev: 1



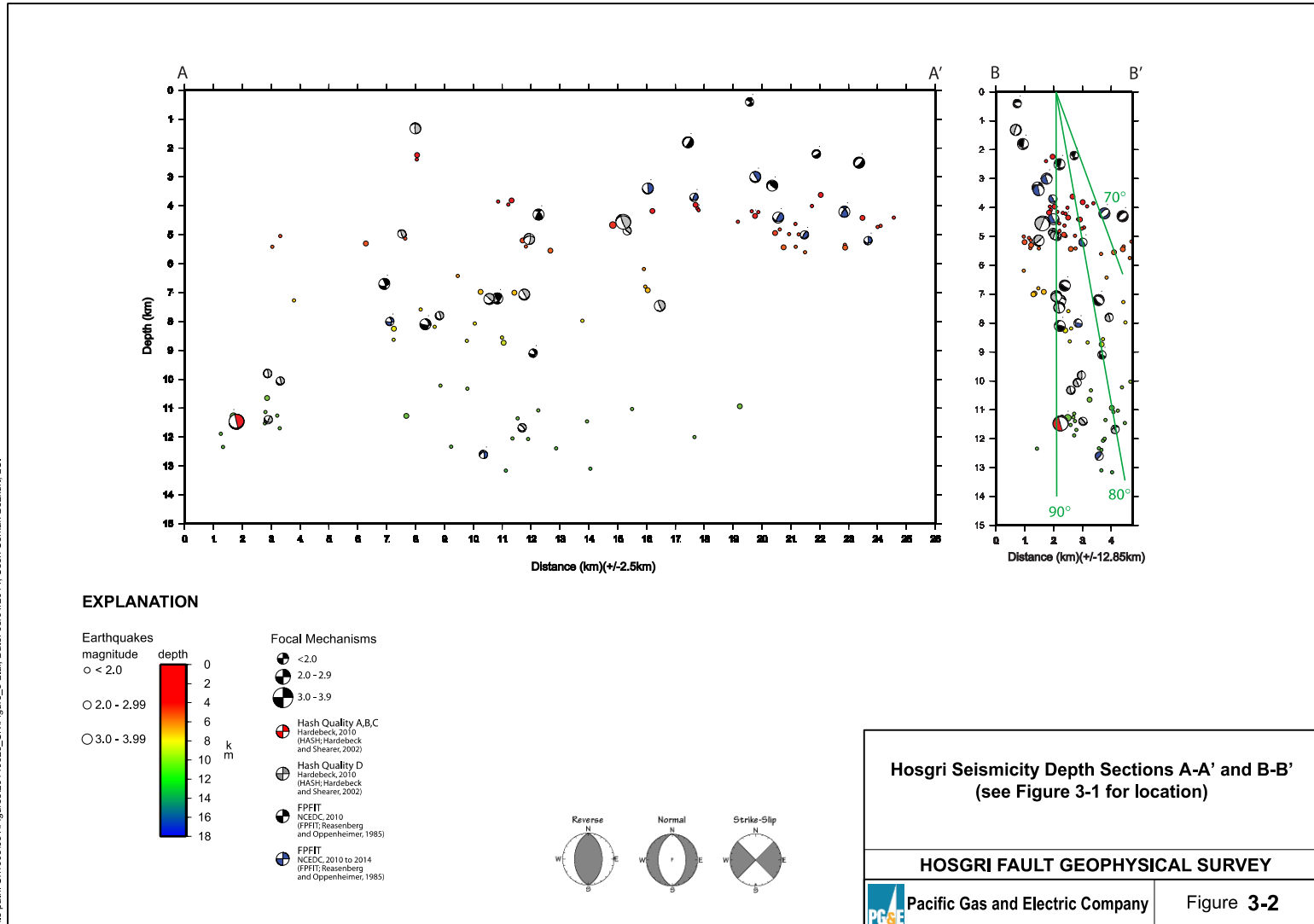
File path: S:\1005051\Figures\20140625\_SNI\Figure\_2-02.mxd; Date: 07/31/2014; User: Serkan Bozkurt, LCI; Rev. 1



File path: S:\10051051\Figures\20140625\_SMF\Figure\_2-03.mxd; Date: 07/31/2014; User: Serkan Bozkurt, LC; Rev: 1

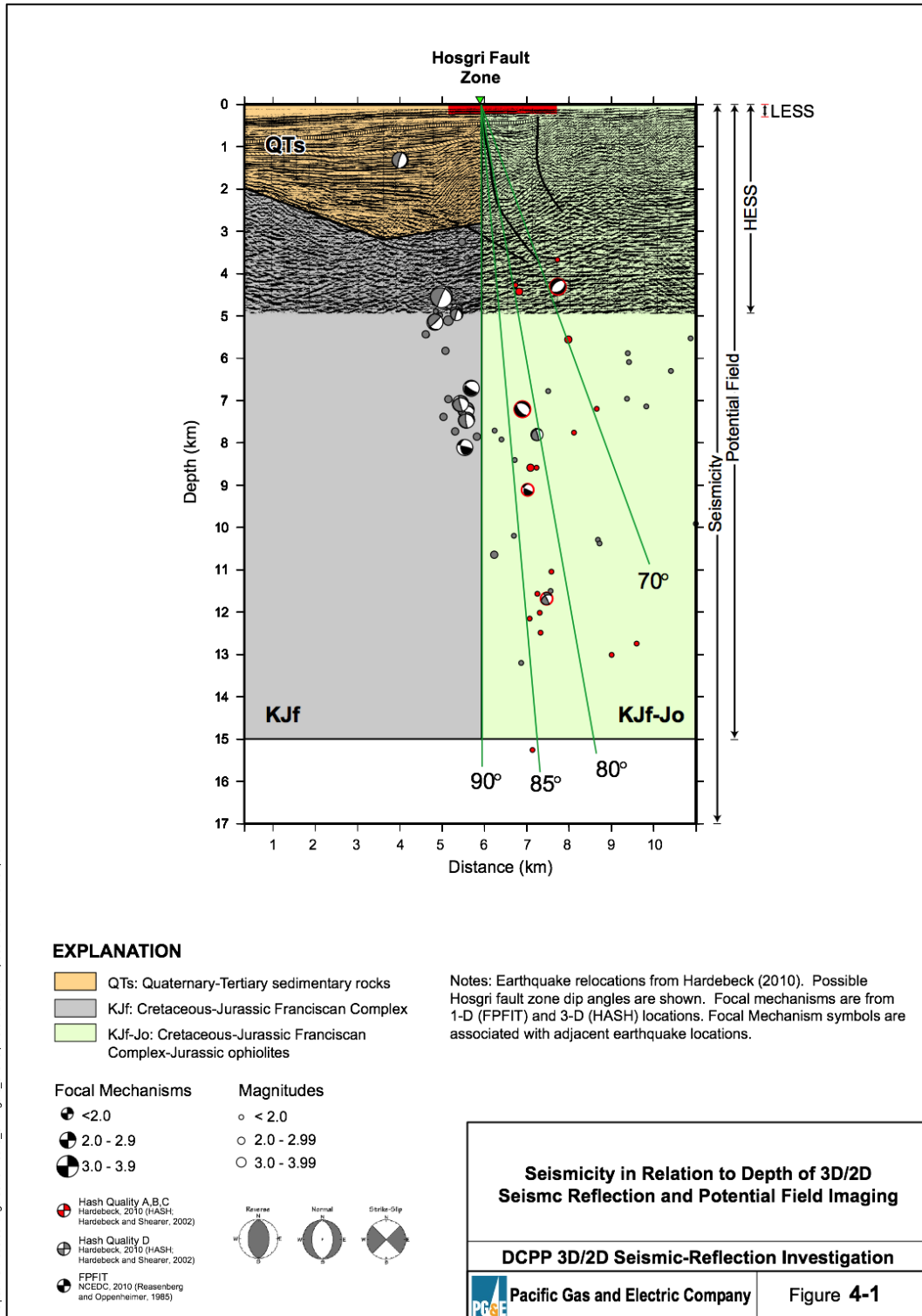


File path: S:\10050051\Figures\20140625\_SNI\Figure\_3-1.ai; Date: 08/05/2014; User: Serkan Bozkurt, LCI



File path: S:\10090651\Figures\20140625\_SNI\Figure\_3-2.ai; Date: 08/01/2014; User: Serkan Bozkurt, LCI





File path: S:\1\05\051\Figures\2014\06\25\_SNI\Figure\_0401.ai; Date: 08/05/2014; User: Serkan Bozkurt, LCI